ABSTRACT

Title of Document:	LIPID-HYDROGEL NANOPARTICLES: SYNTHESIS METHODS AND CHARACTERIZATION
	Jennifer S Hong, Doctor of Philosophy, 2009
Directed By:	Professor Srinivasa R. Raghavan, Department of Chemical and Biomolecular Engineering

This dissertation focuses on the directed self-assembly of nanoscale soft matter particles using methods based on liposome-templating. Nanoscale liposomes, nano-sized hydrogel particles ("nanogels"), and hybrids of the two have enormous potential as carriers in drug delivery and nanotoxicity studies, and as nanovials for enzyme encapsulation and single molecule studies. Our goal is to develop assembly methods that produce stable nanogels or hybrid lipid-polymer nanoparticles, using liposomes as size and shape templates.

First we describe a bulk method that employs liposomes to template relatively monodisperse nanogels composed of the biopolymer, alginate, which is a favorable material for nanogel formation because it uses a gentle ionic crosslinking mechanism that is suitable for the encapsulation of cells and biomolecules. Liposomes encapsulating sodium alginate are suspended in aqueous buffer containing calcium chloride, and thermal permeabilization of the lipid membrane facilitates transmembrane diffusion of Ca^{2+} ions from the surrounding buffer into the

intraliposomal space, ionically crosslinking the liposome core. Subsequent lipid removal results in bare calcium alginate nanogels with a size distribution consistent with that of their liposome template.

The second part of our study investigates the potential for microfluidic-directed formation of lipid-alginate hybrid nanoparticles by adapting the above bulk self-assembly procedure within a microfluidic device. Specifically we investigated the size control of alginate nanogel self-assembly under different flow conditions and concentrations.

Finally, we investigate the microfluidic directed self-assembly of lipid-polymer hybrid nanoparticles, using phospholipids and an N-isopropylacrylamide monomer as the liposome and hydrogel precursors, respectively. Microfluidic hydrodynamic focusing is used to control the convective-diffusive mixing of the two miscible nanoparticle precursor solutions to form nanoscale vesicles with encapsulated hydrogel precursor. The encapsulated hydrogel precursor is polymerized off-chip and the resultant hybrid nanoparticle size distributions are highly monodisperse and precisely controlled across a broad range relevant to the targeted delivery and controlled release of encapsulated therapeutic agents. Given the ability to modify liposome size and surface properties by altering the lipid components and the many polymers of current interest for nanoparticle synthesis, this approach could be adapted for a variety of hybrid nanoparticle systems.

LIPID-HYDROGEL NANOPARTICLES: SYNTHESIS METHODS AND CHARACTERIZATION

By

Jennifer S Hong

Dissertation submitted to the Faculty of the Graduate School of the
University of Maryland, College Park, in partial fulfillment
of the requirements for the degree of
Doctor of Philosophy
2009

Advisory Committee:
Prof. Srinivasa R. Raghavan, Dept. of Chemical and Biomolecular Engineering, Chair
Prof. Helim Aranda-Espinoza, Dept. of Bioengineering
Prof. John P. Fisher, Dept. of Bioengineering
Prof. Robert M. Briber, Dept. of Materials Science and Eng., Dean's Representative
Adjunct Asst. Prof. Michael Gaitan, Dept. of Bioengineering

DEDICATION

This work is dedicated to my parents for their undying support and love. I could not have done this without the both of you always standing by my side.

ACKNOWLEDGEMENTS

First of all, I would like to extend my sincerest gratitude to Dr. Srinivasa Raghavan, my advisor at the University of Maryland, for his continuous guidance and patience throughout my dissertation research. I have learned so much and have had an enriching experience by being a member of his Complex Fluids Group.

I also would like to thank my advisor in the Semiconductor Electronics Division (SED) at the National Institute of Standard and Technology (NIST), Dr. Michael Gaitan, for providing me with a great deal of guidance and technical advice over the past few years. I am also very thankful for the encouragement and support from my friends and colleagues at NIST, especially Dr. Laurie Locascio, Dr. Jon Geist, Dr. Darwin Reyes, Dr. Jayna Shah, Dr. Samuel Stavis, and Geraldine Mijares.

To the students in the Complex Fluids Group, I am grateful to have had the opportunity to share ideas and partake in interesting discussions at our weekly meetings. I would also like to thank my friends in the Bioengineering Graduate program for their advice and support.

Finally, I am extremely appreciative for my family and friends who have given me so much moral support and encouragement during my graduate career. You have helped me more than I can possibly express in words.

TABLE OF CONTENTS

LIST OF FIGURES

1. INTRODUCTION AND OVERVIEW

1.1 PROBLEM DESCRIPTION AND MOTIVATION

This dissertation is focused on the templated assembly, characterization, and applications of soft nanoparticles derived from liposome and hydrogel precursors. Recently, the field of supramolecular chemistry has attracted increasing exploration. In particular, researchers have been applying the concept of self-assembly to develop new nano-based materials, constructing them from simple molecular building blocks via noncovalent (e.g. hydrophobic, electrostatic, hydrogen bonding) interactions[2-4]. Nanoparticles are currently a central research interest in biomedical, optical, and electronic fields due to their unique properties owing to their small size, high surface to volume ratio, and chemical composition[5,6]. As a result, new classes of nanoparticles are continuously being investigated and developed to address the delivery needs for various biological applications. A major barrier preventing the practical application of many nanoparticles is the lack of methods that can produce uniform populations in a relatively simple and reproducible manner. This problem is most prevalent in clinical and toxicological studies, where accurate data concerning the physiological and environmental effects of nano-sized carriers is desperately needed[6,7], but limited knowledge exists due to the differences between the preparation techniques applied.

Nanoscale liposomes, well recognized for their drug delivery potential and utility, possess useful surface properties for adhering targeting moieties and stealth

molecules, and provide a relatively impermeable barrier in terms of controlled release. However, the lipid bilayer is extremely susceptible to perturbations due to environmental changes in temperature, pH, or osmolarity, which is a disadvantage in therapeutics when considering the need for sustained release and prolonged circulation in the body. Hydrogel nanoparticles offer greater mechanical stability compared to liposomes, and the three-dimensional structure offers a level of control for the release of an encapsulated biomolecule, but they are prone to degradation and aggregation, and lack the targeting properties of liposomes[8].

The intricate biological parameters that must be considered when designing a particulate delivery system has caused a natural progression towards the development of more complex hybrid nanoparticle systems that combine the advantages of multiple soft matter materials to produce more robust and versatile nanocarriers[9]. In particular, by combining the liposome and hydrogel components, the resultant lipid-polymer hybrid nanoparticles are equipped with the strengths of each of the single material systems while compensating for each of their weaknesses. Such hybrid nanoparticles are increasingly becoming the focus of synthesis and characterization studies, due to their potential practical utility in drug delivery and life sciences research[9,10].

Lipid-polymer nanoparticles have been synthesized using bulk self-assembly methods. One of the common bulk methods is to first synthesize the hydrogel nanoparticle and thereafter assemble the lipid coating around the nanogels to produce

the hybrid nanoparticles[11,12]. A second method involves the use of liposomes as reaction vessels for the formation of the hydrogel core component. Several groups have applied the latter method in bulk, using various lipid formulations and polymerization techniques, the majority of which have applied free radical polymerization of liposomes encapsulating synthetic monomers, crosslinking molecules with a low molecular weight, and photoinitiator formulations to form solid cores[13-16]. Alternative approaches for hybrid nanoparticle formation include nanoprecipitation[9] and solvent injection techniques.

Beyond these bulk synthesis methods, relatively few microfluidic systems have been reported for the self-assembly of more complex hybrid nanoparticle systems, though they have been demonstrated to improve control over the continuous self-assembly of single material polymeric and phospholipid nanoparticles[17-19] compared with bulk liposome preparation methods. There is a need for similar reliable and simple synthesis methods that enable precise control over the self-assembly of lipid-hydrogel hybrid nanoparticles, as their more complex structures generally require more elaborate synthesis methods[5,20]. As nanoparticle size and shape are two critical properties that strongly affect the biological fate or toxicity of a particular carrier[5,21], methods that produce homogeneous and versatile nanoparticle systems using simple and preferably automated processes are necessary for working towards promoting greater consistency across laboratories.

1.2 OUR APPROACH

Our goal is to develop synthesis methods that demonstrate size and structure control over the resultant nanoparticle populations, and to this end we implement liposomes as nanotemplates for the self-assembly of hydrogel and hybrid lipid-polymer nanoparticles using both bulk and microfluidic methods. Chapter 2 describes properties of the hydrogel and liposome components we have investigated, and discusses the nanogel characterization techniques we have used: asymmetric-flow-field-flow-fractionation (AF4), multi-angle light scattering (MALLS), transmission electron microscopy (TEM), and dynamic light scattering (DLS).

1.2.1. Liposome-Templated Alginate Nanogels

In Chapter 3, we present a study on bulk liposome-templated formation and characterization of relatively monodisperse calcium alginate nanogels. Here, the cores of nanoscale liposomes are employed as reaction vessels to template the supramolecular assembly of calcium alginate nanogels. For our experiments, liposomes composed of a formulation with a high bilayer melting temperature (T_m) are formed with sodium alginate encapsulated within and suspended in an aqueous buffer containing calcium chloride. The transmembrane diffusion of divalent calcium ions into the liposomal core to crosslink the encapsulated alginate chains is mediated by heating the sample to temperatures in the vicinity of the T_m, at which point transbilayer permeability is known to be increased. Subsequently, the lipid bilayer covering the gel is removed by addition of a detergent. The resulting alginate gels have a size distribution consistent with that of the template liposomes (~120-200 nm),

as confirmed by TEM and MALLS coupled with AF4. We have synthesized nanogels of different average sizes by varying the template dimensions, and have demonstrated that the gel size can be further tuned after synthesis by the addition of monovalent salt to the solution.

1.2.2. Microfluidic Directed Assembly of Alginate Nanogels

Chapter 4 focuses on developing a microfluidic analogue of the method described in Chapter 3. We attempted to use microfluidics for the self-assembly of liposomes and simultaneous encapsulation of sodium alginate. The approach relies on diffusion between two miscible streams, and has been demonstrated previously in our laboratory to synthesize monodisperse liposome populations[22]. Using modified formulations of the lipid and alginate, we were able to control the size distributions of the resultant liposome populations by changing the microfluidic mixing conditions. These liposomes were generally smaller compared to those synthesized by the bulk method in Chapter 3. However, probably due to the smaller size, the encapsulation efficiency of alginate in these liposomes was found to be quite low, and consequently the ionic crosslinking of the liposome core was not pursued. Although this microfluidic approach proved challenging to implement for larger polymers such as alginate, we believe it is applicable to hybrid nanoparticle systems where the hydrogel component is based on oligomer or monomer precursor molecules.

1.2.3. Microfluidic Directed Assembly of Lipid-Hydrogel Hybrid Nanoparticles

In Chapter 5, we present a microfluidic method to direct the formation of lipid-hydrogel hybrid nanoparticles of engineered size using a monomeric precursor for hydrogels. This method utilizes hydrodynamic focusing to precisely control the convective-diffusive mixing of two miscible solutions (a cholesterol/phospholipid formulation in isopropanol, and a monomer/crosslinker solution in aqueous buffer), forming nanoscale lipid vesicles with encapsulated hydrogel precursors. These precursor nanoparticles are collected off-chip and UV-irradiated to crosslink the liquid cores into hydrogels. Nanoparticles with low polydispersities (3 to 5%) can be prepared with average diameters in the 150 to 300 nm range. These size distributions and structural properties are highly relevant to the targeted delivery and controlled release of encapsulated therapeutic agents. This method may be extended to the directed self-assembly of other hybrid nanoparticle systems with engineered size/structure-function relationships to advance the success of soft nanoparticles for practical use in healthcare and life science applications.

Ultimately we believe that microfluidics will offer a more automated and controlled nanoparticle manufacturing process, as well as allow us to explore a range of formation conditions more systematically and efficiently than can be accomplished through bulk preparation methods. The application of microfluidics to nanoparticle formation has the potential to become a standardized approach to control nanoparticle synthesis processes and to increase our understanding of the various factors that affect their assembly behavior.

2. BACKGROUND

2.1. ALGINATE

Sodium alginate is linear unbranched bio-copolymer composed of 1,4-linked β-D-mannuronic (M) (Figure 2.1a) and α-L-guluronic (G) (Figure 2.1b) residues that can be ionically crosslinked by divalent cations (e.g. Ca^{2+}, Ba^{2+}, Sr^{2+}) to form a hydrogel. This crosslinking of adjacent polymer chains occurs via the exchange of monovalent sodium ions from the guluronic residues with divalent cations, thus forming a gel network described by the "egg-box" model.[23]

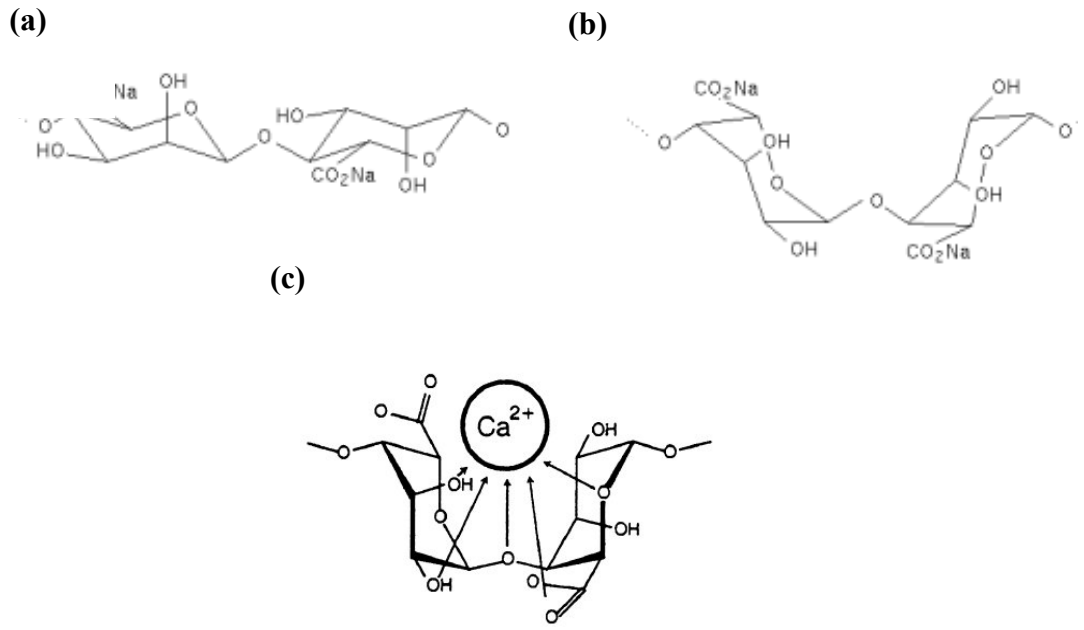

Figure 2.1. Structure of (a) β-D-mannuronic (M) and (b) α-L-guluronic (G) residues in a sodium alginate polymer. The ionic coordination of the G residues with divalent Ca^{2+} is illustrated in (c).[1]

Alginate is appealing as an in situ forming biomaterial because it is inert by nature, has a gentle reversible crosslinking mechanism, and its gel properties may be customized based on M/G ratios[24,25]. Alginate is also referred to as a "smart" responsive polymer because its gel network is the result of non-covalent (i.e. physical) crosslinking. It has been shown that changes in monovalent cation concentration and pH can cause alginate gels to swell or shrink due to ionic interactions with the alginate acid residues[26,27]. Though alginate was traditionally used as an emulsifier or stabilizer in the food industry, recently it has been applied as a controlled release material in drug delivery systems,[28-30] and as favorable matrix for cell encapsulation and tissue repair in tissue engineering[25,31-33].

2.2. LIPOSOMES

Molecular self-assembly is ever-present in biological systems, where molecules spontaneously aggregate into dynamic complex structures, such as phospholipids assembling into cell membranes, or actin monomers organizing into microfilaments[34,35]. Liposomes are well-known self-assembled models of the cell membrane that spontaneously form in aqueous environments by the organization of amphiphilic molecules into closed spherical bilayer structures, where the hydrophilic head groups prefer to be in contact with water and the hydrophobic tails preferred to be shielded inward, as shown in Figure 2.2.

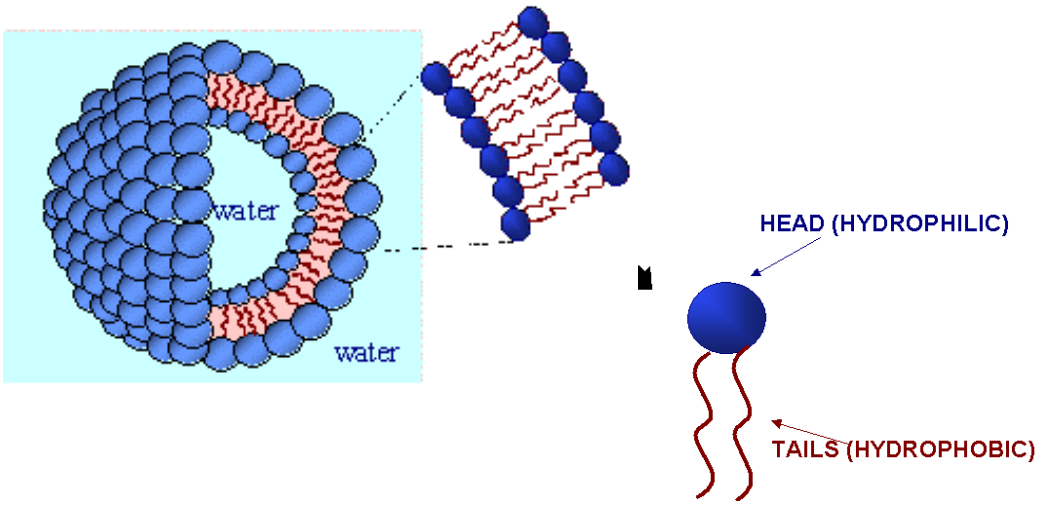

Figure 2.2. Schematic of a liposome, with the hydrophilic head groups (blue) facing the water, and the hydrophobic tail groups (red) buried within the bilayer.

Self-assembly is thermodynamically driven, where the system acts to minimize its Gibbs free energy in the process. For this system, the liposome structure is favored mainly due to an increase in the entropy of water molecules due to the hydrophobic tails being hidden in the bilayer, which is known as the hydrophobic effect. Upon formation, liposomes can encapsulate and sequester compounds from the aqueous environment into its interior while preserving their functionality. This ability has made liposomes extremely attractive as carriers for a wide host of biological applications.[36-38]

A well-known characteristic of lipid bilayers is their greatly increased permeability to small reagents at temperatures near their lipid chain melting temperature, T_m. As shown in Figure 2.3, at temperatures below the T_m the bilayer is in the gel (L_β) phase, where the hydrophobic tails of the lipid molecules are elongated

and rigid; at temperatures above the T_m, the lipid molecules exist in the liquid crystalline (L_α) phase, where the tails are more fluid.

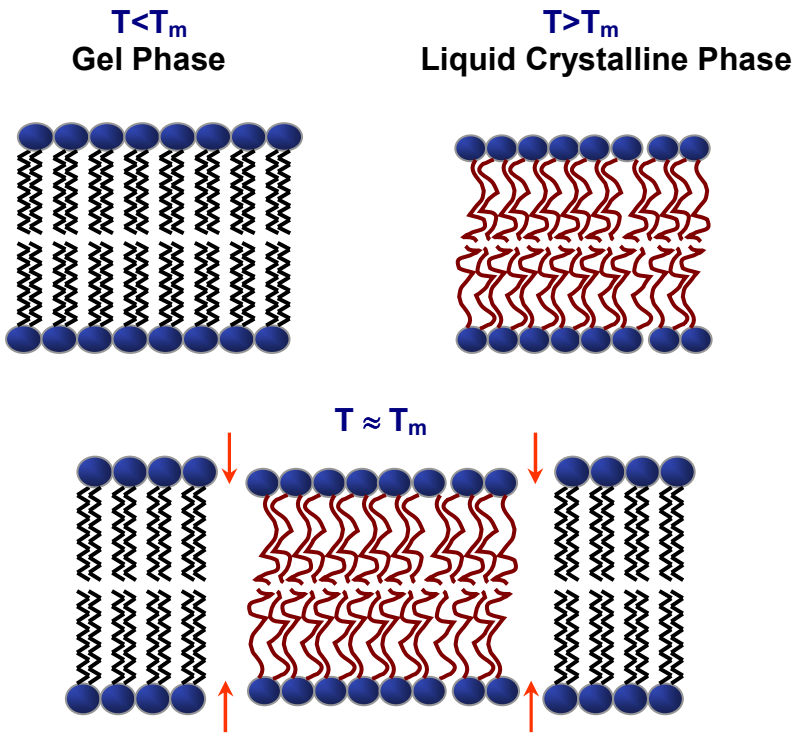

Figure 2.3. Temperature effects on bilayer permeability with respect to the lipid chain melting temperature, T_m. The red arrows illustrate packing discontinuities.

In either state, lipid tail packing is continuous and the bilayer membrane is relatively impermeable to small molecules. However, near the T_m, there is a coexistence of the two phases which causes packing discontinuities at the gel-liquid crystalline interfaces, and thus transmembrane permeability increases[39-42]. This property can be used as a trigger for facilitating diffusion of substrates into the liposome interior, or conversely, for releasing encapsulated agents to the exterior[39,43].

2.3. POLY(N-ISOPROPYLACRYLAMIDE)

Poly(N-Isopropylacrylamide) (PNIPA) is perhaps the most widely studied thermally responsive "smart" polymer in controlled release and drug delivery[44,45]. As shown in Figure 2.4 the precursor monomer, N-isopropylacrylamide (NIPA) mixed with a small amount of crosslinking monomer, N,N'-Methylene-bis-acrylamide (MBA) and photoinitiator diethoxyacetophenone (DEAP) can be polymerized via UV free radical polymerization into a hydrogel that has a characteristic low critical solution temperature of approximately 32 °C[46,47].

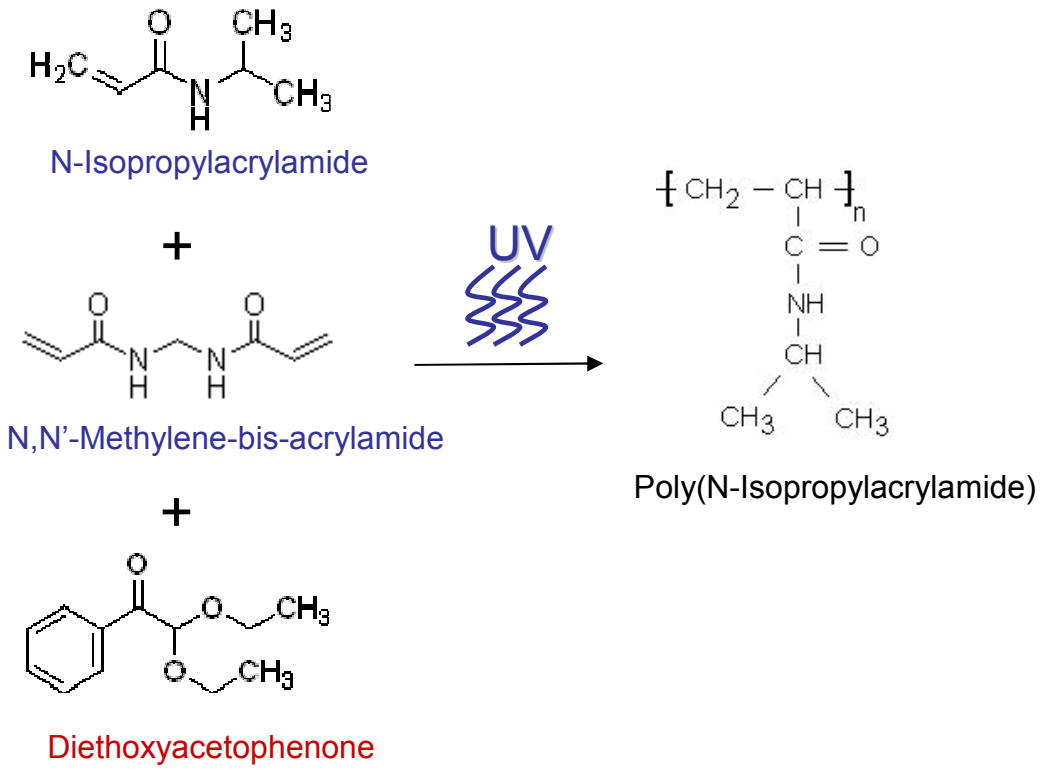

Figure 2.4. A hydrogel precursor solution of monomer N-isopropylacrylamide (NIPA), crosslinking monomer N,N'-Methylene-bis-acrylamide (MBA), and photo-initiator diethoxyacetophenone (DEAP) can be polymerized by UV irradiation into a thermally sensitive poly(N-isopropylacrylamide) (PNIPA) gel.

At temperatures below the LCST (Figure 2.5), PNIPA is soluble in aqueous solutions and its hydrogels are known to swell; conversely as the temperatures above the LCST, the polymer chains phase separate and PNIPA hydrogels collapse. This drastic transition occurs due to increasing polymer-polymer hydrophobic interactions and the disruption of hydrogen bonded water molecules around the amide group of the polymer side chains[45].

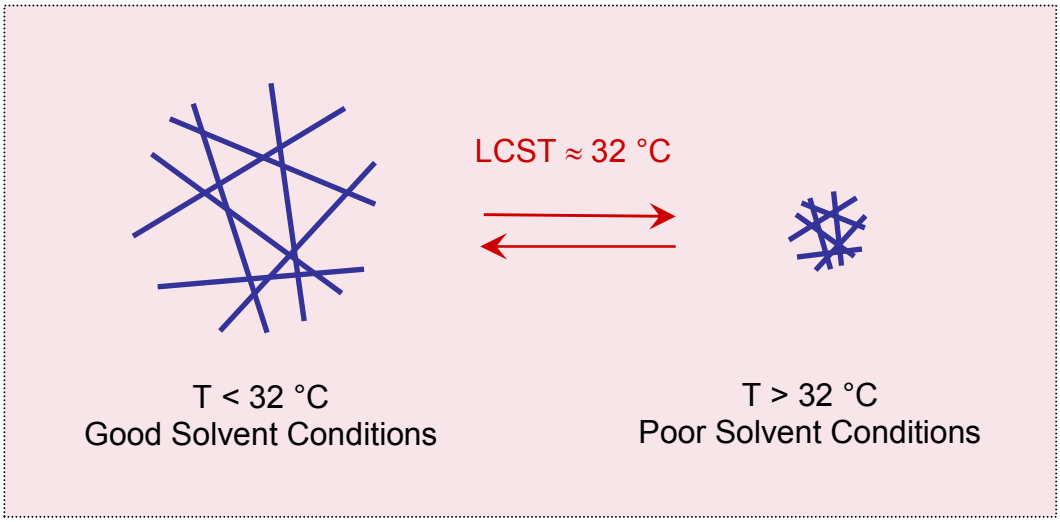

Figure 2.5. PNIPA has an LCST of approximately 32 °C, below which the polymer is in a hydrated state and above which the polymer collapses.

PNIPA has been extensively characterized and is used in many nanoparticle formulations as a core or shell material for controlled release studies[48]. PNIPA is soluble in water at room temperature but phase separates at the physiological temperature (37 °C), making it an appealing material for therapeutic applications. Modification of the polymer such as addition of a co-monomer to the precursor solution prior to polymerization, or addition of other components following

polymerization can alter the properties of the hydrogel and shift the LCST[49], making it an extremely versatile material with an adjustable trigger[21].

2.4. MICROFLUIDICS

Since its inception dating back 25 years, microfluidics has become an area of ever-growing interest, where the goal is to integrate processes of a chemical or biochemical analysis and miniaturize them onto a small microchip device, or lab-on-a-chip. Such a system offers many advantages over traditional bulk analyses: low cost of device fabrication, very low consumption of sample and reagent volumes, portable size, shorter sampling times, and reproducibility of mixing condition.[50].

In general, channels in microfluidic devices have height or width dimensions of less than 200 μm and possess unique fluidic properties owing to their micron size scales. Due to dominating viscous forces at such small channel dimensions, aqueous flow in microchannels is typically laminar[51], and therefore two aqueous streams flowing parallel to each other in the same direction have a predictable interfacial region where the mixing is predominantly governed by molecular diffusion (i.e. Brownian motion)[52-54]. As such, small molecules and ions with a higher diffusion coefficient diffuse more rapidly between streams, while larger particles diffuse more slowly. The ability to regulate these liquid interfaces by controlling flow rates allows increased control over assembly processes compared to bulk systems, which are affected by unpredictable turbulent flow conditions and chaotic mixing.[55]

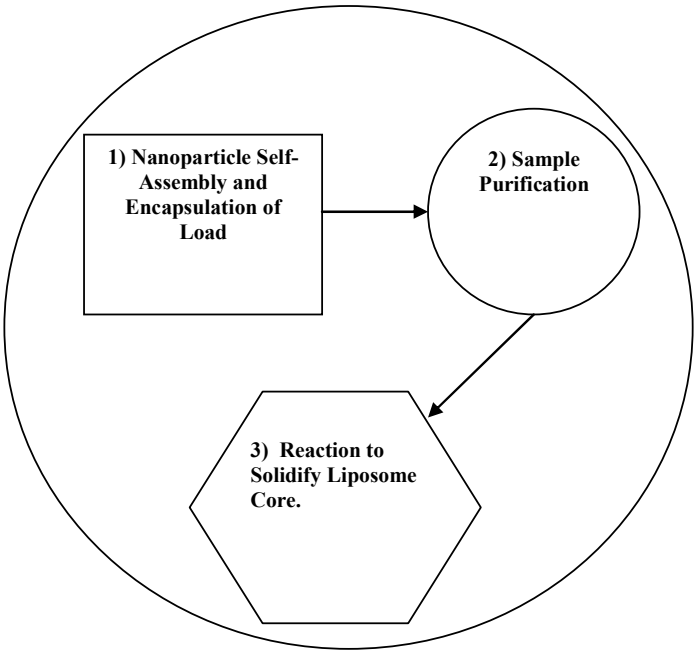

Figure 2.6. Schematic of long-term goal for automated formations of hybrid soft matter nanoparticles.

The ultimate goal for a microfluidic system geared towards hybrid nanoparticle formation, as shown in Figure 2.6, is to integrate the directed assembly, encapsulation, purification, and reaction steps in a single continuous-flow device. However, as in many microfluidic assays that involve multiple steps, integration is the most difficult challenge. Therefore, our work is focused primarily on liposome formation and hydrogel precursor encapsulation within a microfluidic device in order to understand the effects on the self-assembly aspect of synthesis, which is perhaps the most critical step affecting the homogeneity of nanoparticle populations.

We have applied a method developed at the National Institute of Standards and Technology (NIST) that uses a continuous-flow method to produce monodisperse

liposome populations by means of hydrodynamically focusing a stream of lipid solution at a microchannel cross-junction between two aqueous streams[22,55].

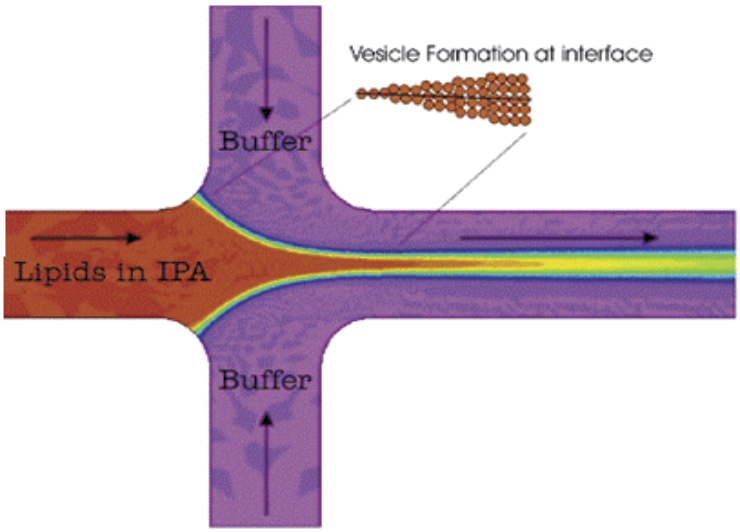

Figure 2.7. Hydrodynamic focusing of lipids in IPA leads to liposomes at the IPA/buffer interface.[55]

As shown in Figure 2.7, as the miscible alcohol/lipid and aqueous buffer streams meet at the interface, the lipids become less soluble and eventually self-assemble at a critical alcohol to water ratio, simultaneously encapsulating the surrounding aqueous solution during formation. Adjusting the degree of hydrodynamic focusing through the ratio of the volumetric flow rate (VFRR) of the buffer (Q_{buffer}) to that of the lipid-solvent (Q_{lipid}), changes the microfluidic mixing conditions and enables the self-assembly of highly uniform liposomes with average diameters ranging from 40 to 100 nm. This method is much simpler than alternate sizing methods for liposomes such as extrusion or sonication.

2.5. CHARACTERIZATION TECHNIQUES

2.5.1. Asymmetric Flow Field-Flow Fractionation (AF4)

The basic principle of AF4 is to separate species based on their diffusion coefficients in a flow separation channel (100-500 μm thickness depending on channel spacer) with a very thin laminar flow, as illustrated in Figure 2.8.

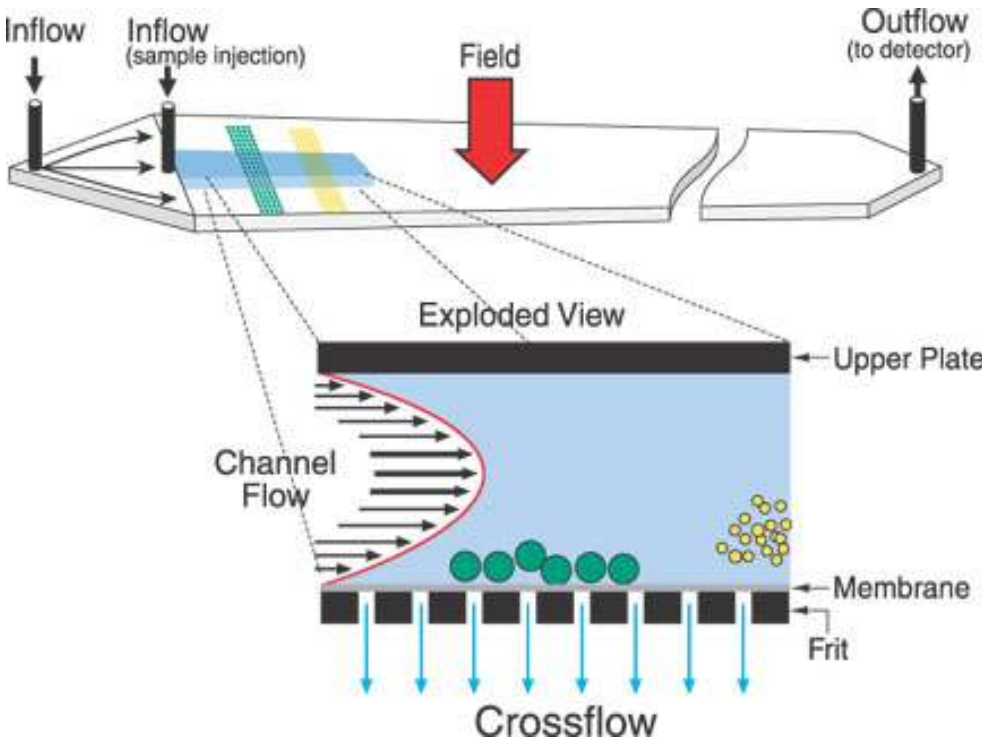

Figure 2.8. Schematic of AF4 separation channel from Wyatt Technology.

The upper plate of the channel is impermeable while the bottom channel plate, made of a porous frit material, is permeable. The bottom plate is covered with a filtration membrane with a typical cutoff size of 10 kDa, which serves to prevent the

sample from exiting the separation channel. The channel has a parabolic flow profile of the carrier buffer solution, and simultaneously with injection of the sample, a crossflow is applied perpendicular to the carrier flow to focus the sample against the semi-permeable accumulation membrane at the bottom of the channel inlet. As the crossflow is gradually reduced, smaller particles reach equilibrium between diffusion (i.e. Brownian motion of the particle) and the force of the perpendicular crossflow farther above the accumulation wall, where the channel flow is faster. Thus, separation occurs as smaller particles, which have larger diffusion coefficients, elute first with larger particles, which have slower diffusion coefficients, following later.

The eluting sample can then be directly coupled to a light scattering instrument to obtain real-time data from each elution slice, resulting in a more accurate size distribution measurement. Separation prior to light scattering lessens the potential of larger particles (e.g. dust, aggregates, polydispersity) to skew the average size data towards larger values, which is known to occur when applying batch dynamic light scattering (DLS) techniques to a sample in scintillation vial.[56]

The AF4 technique is analogous to size-exclusion chromatography (SEC), but with some advantages. Unlike SEC, which uses a column loaded with a separation medium that may interact with and degrade the sample of interest, AF4 has no need of a stationary phase, thus offering a gentler means of separation.

2.5.2. Multi-Angle Laser Light Scattering (MALLS)

Scattering techniques are indispensable for characterizing nanoparticle size, as size is considered a major factor in influencing particle efficiency and function. MALLS, also known as static light scattering, measures the intensity of scattered light from a sample as a function of angle from the incident beam of light (Figure 2.9).

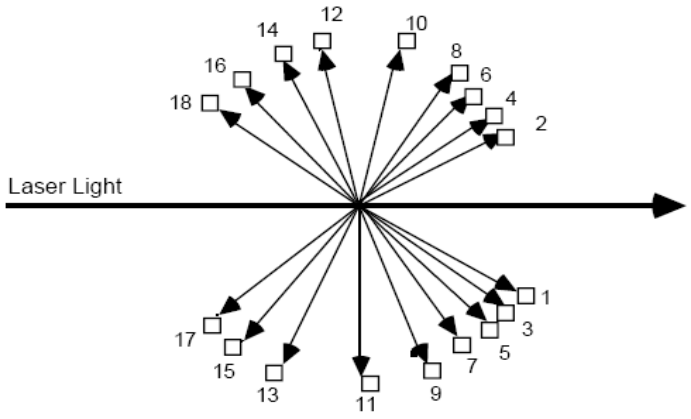

Figure 2.9. Schematic of MALLS where scattered light from the incident light beam is measured by detectors located at fixed angles around the sample.

For colloids, MALLS data is used to determine the radius of gyration R_g, which is the root mean square of mass-weighted distances of the particle's sub-volumes from its center of mass. The equations for determining R_g are further explained in Section 3.2.

2.5.3. Dynamic Light Scattering (DLS)

Dynamic light scattering (DLS), also known as quasi elastic light scattering (QELS), probes the Brownian motion of particles in a fluid by measuring the fluctuating intensity of light scattered from a sample at a certain angle θ. The fluctuations are processed by applying an autocorrelation function $g^{(2)}(q,\tau)$ vs. the correlation time τ.

$$g^{(2)}(q,\tau) = \frac{\langle I(q,t)I(q,t+\tau)\rangle}{\langle I(q,t)^2\rangle} \tag{2.1}$$

For light scattering the wave vector q is defined as:

$$q = \frac{4\pi n}{\lambda}\sin\left(\frac{\theta}{2}\right) \tag{2.2}$$

where n is the refractive index of the sample solvent.

The second order intensity autocorrelation function $g^{(2)}(q,\tau)$ can be converted to an electric field autocorrelation function $g^{(1)}(q,\tau)$ using the Siegert relation:

$$g^{(2)}(q,\tau) = 1 + f\left|g^{(1)}(q,\tau)\right|^2 \tag{2.3}$$

where f is an adjustable parameter that depends on the instrument geometry. For dilute monodisperse spherical particles, the electric-field autocorrelation function is a single exponential decay that is determined by the translational diffusion coefficient of the particles D:

$$g^{(1)}(q,\tau) = \exp(-Dq^2\tau) \tag{2.4}$$

The diffusion coefficient is then used to obtain the particle size using the Stokes-Einstein equation:

$$D = \frac{k_B T}{6\pi\eta R_h} \tag{2.5}$$

where k_B is the Boltzmann constant, T is the absolute temperature and η is the viscosity of the solvent. DLS outputs the hydrodynamic radius R_h of the sample, which is the radius of the bare particle along with any solvation layer.

2.5.4. Transmission Electron Microscopy (TEM)

Transmission Electron Microscopy (TEM) is an imaging technique that transmits a beam of electrons through a sample deposited on a thin film. Electrons that collide with the sample are deflected while unscattered electrons pass through. An image is formed from the differences in transmitted electron intensity, and shows the structure and shape of the sample. TEM is often done in parallel with light scattering for nanoparticle characterization as a qualitative check for the quantitative size information obtained via light scattering measurements.

Hollow core vesicles typically require negative staining prior to placing sample on a TEM grid in order to achieve sufficient contrast to resolve the bilayer membrane[57]. Solid nanoparticles or nanogels will inherently scatter more electrons due to the solid composition, and thus do not require staining although it can improve image contrast.

3. LIPOSOME-TEMPLATED ALGINATE NANOGELS*

*The results presented in this chapter have been published in the following journal article: Jennifer S. Hong, Wyatt N. Vreeland, Silvia H. DePaoli Lacerda, Laurie E. Locascio, Michael Gaitan, and Srinivasa R. Raghavan, *"Liposome-templated Supramolecular Assembly of Responsive Alginate Nanogels."* Langmuir, **24**, 4092-4096 **(2008)**.

3.1. INTRODUCTION

Polymer hydrogels, i.e., three-dimensional networks of polymer chains swollen in water, are ubiquitous in biology as well as in technology. Such hydrogels have long been envisioned as a means of storing an active ingredient, such as a therapeutic drug, flavor molecule, cosmetic ingredient, or agrochemical, and slowly releasing these molecules into the surrounding environment[58-60]. For example, hydrogels made of synthetic degradable polymers have been used in medicine as implantable drug delivery vehicles[61-63]. In many emerging biomedical applications, the size of the hydrogel is turning out to be an important control variable. For instance, gel particles smaller than about 200 nm can evade capture by macrophages in the bloodstream, and are thus more likely to remain in circulation for longer times compared to larger particles[36,37]. For cancer therapy also, gels ranging in size from about 100 to 200 nm could be particularly useful since these could penetrate into the vasculature of many tumors[64-67]. Thus, a need exists for small hydrogel particles in the nanoscale size regime.

In this Chapter, we describe the formation of nanosized gels using lipid vesicles (liposomes) as a template. As is well-known, liposomes are closed structures formed by the self-assembly of amphiphilic lipid molecules in water, with the lipids organized at the liposomal shell in the form of a bilayer membrane. We employ the cores of nanosized liposomes as reaction vessels within which we induce the gelation of the biopolymer, sodium alginate under the action of divalent calcium ions. The gelation transforms the liposomal interior from a fluid state to a soft, elastic solid. Upon removal of the lipid bilayer covering the gelled core, we are left with alginate nanogel particles that closely match the size of the liposomal template. We characterize our nanogels by both optical or electron microscopy as well as light scattering. A light scattering technique coupled with field-flow fractionation allows us to precisely compare the size distributions of the liposomes and the templated nanogels[68,69]. The data show that our synthesis scheme corresponds to a true templating reaction, and that our procedure can be extended to preparing nanogels of different sizes and chemistries. Moreover, these alginate nanogels can be subsequently reconstituted as stable dispersions in water or buffer solutions.

Several earlier studies have reported gel synthesis using liposomes as templates[8,10,14,15,70,71], although in most of these cases the focus was on relatively large gel particles. Only one group has systematically studied the synthesis of nanosized gels via liposomal templates. Those gels were based on the synthetic polymer, poly(N-isopropylacrylamide) (PNIPA)[13,72,73]. Our interest in this study is on ionically crosslinked biopolymer nanogels, and the emphasis of the present work is

on improvement and detailed characterization of the templating process of such gels within liposomes.

To improve the templating process, our approach is to use a trigger mechanism to initiate crosslinking within our liposomal cores. We exploit a well-known property of lipid bilayers, which is that the bilayers become more permeable close to their bilayer melting temperature T_m[39,40,42,74]. The increased permeability arises because near T_m, the bilayer exhibits a co-existence of "gel" domains (in which the lipid tails are elongated and rigid) and liquid crystalline domains (where the lipid tails are fluid). Between these domains, there are grain boundaries, which causes the formation of pores in the membrane, in turn leading to an increase in transmembrane permeability. Here, we use lipids that have a T_m above room temperature to form our liposomes, and we encapsulate sodium alginate in these liposomes (Figure 3.1). Thereafter, we introduce Ca^{2+} ions into the solution, and we raise the temperature to the T_m. Thereby, we facilitate the diffusion of Ca^{2+} ions into the liposomal core, where the ions crosslink alginate chains at junction zones (this is the well-known "egg-box" mechanism). We have used alginate in our studies because it is appealing as a biomaterial due to its ability to undergo crosslinking under mild conditions[24,25,28].

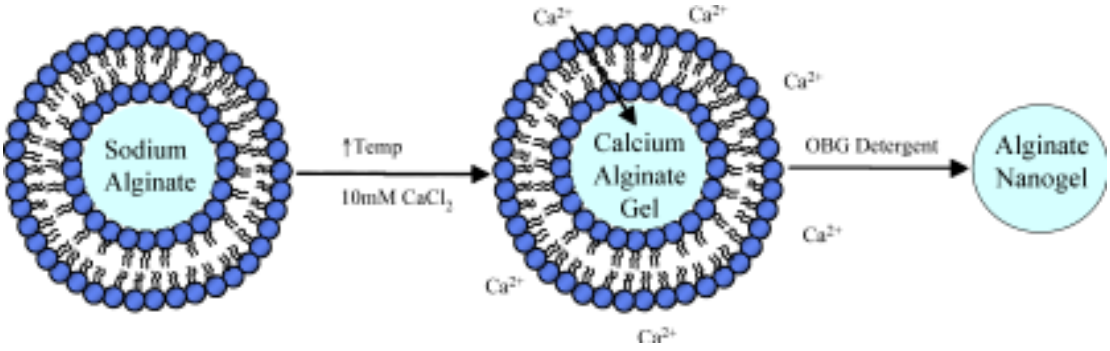

Figure 3.1. Schematic of alginate nanogel synthesis using liposomal templates. Liposomes encapsulating sodium alginate are placed in a 10 mmol/L $CaCl_2$ solution and exposed to temperatures near the T_m of the lipid. The increased transmembrane permeability allows Ca^{2+} to diffuse into the liposomes and ionically crosslink the alginate to form a nanogel. Subsequent removal of the lipid shell yields alginate nanogels.

The ability to gel the cores of liposomes has applications beyond drug delivery. Specifically, it is worth noting that eukaryotic cells can generally be considered as gels enclosed by a bilayer membrane, where the gel is formed by the polymerization of cytoskeletal proteins such as actin, filamin, and tubulin. Thus, a liposome with a gelled core might be a better model for a biological cell compared to a buffer filled liposome[75]. Moreover, a gelled liposome could find applications as a container for single molecule fluorescence studies, e.g., in localizing a single DNA or protein molecule within the interior. These types of fundamental studies will be the focus of future efforts in our lab.

3.2. EXPERIMENTAL SECTION

Materials. The lipid, 1,2-Dipalmitoyl-sn-Glycero-3-Phosphocholine (DPPC, > 99% purity) and cholesterol (> 98% purity) were purchased from Avanti Polar Lipids (Alabaster, AL). Other amphiphiles and chemicals were purchased from Sigma-Aldrich (St. Louis, MO), including the lipid, dicetyl phosphate (DCP), the detergent, octyl-ß-glucopyranoside (OBG), sodium azide (NaN_3), and ethylenediaminetetraacetic acid (EDTA). The alginate biopolymer was also obtained from Sigma-Aldrich and it was a low-viscosity sodium alginic acid, composed primarily of 1-4 β-D-mannuronic acid residues. The molecular weight of the polymer was determined to be around 145 kDa by light scattering (Zimm plot). Salts NaCl and $CaCl_2$ were purchased from Fisher Scientific (Pittsburgh, PA). The buffer ingredients, tris(hydroxymethyl)aminomethane (Tris) from Amresco (Solon, OH) and N-tris(hydroxymethyl)methyl-3-amino-propanesulfonic acid (TAPS) from Midwest Scientific (Valley Park, MO) were used to prepare Tris-TAPS-NaCl buffer (at pH 8.0) by combining 50 mM of Tris and TAPS and 15 mM NaCl. A Tris-TAPS-$CaCl_2$ buffer was also prepared, with the same Tris and TAPS concentrations and combined with 10 mM of $CaCl_2$. 3 mM NaN_3 was added to all buffer solutions to prevent bacterial contamination.

Liposome Preparation. A lipid formulation consisting of DPPC:cholesterol:DCP (7:2:1 molar ratio) was used to prepare liposomes by the solvent injection method[76,77]. This method involved dissolving 5 μmol of the lipid formulation in chloroform and evaporating the solvent under a dry nitrogen stream. The resulting thin lipid film was

placed in a vacuum dessicator overnight to completely remove any residual solvent. The dried lipid film was resolubilized in 50 μL dry isopropyl alcohol (IPA) and was injected into 1 mL of Tris-TAPS-NaCl buffer while vortexing, which yielded control liposomes at a concentration of 5 mM. To prepare liposomes containing the alginate in their cores, the alginate was added to the buffer solution prior to lipid injection. Details on alginate nanogel preparation are given in the Results section. Details on alginate nanogel preparation are given in the Results section.

Light Scattering and Asymmetric Flow Field-Flow Fractionation (AF4). An Eclipse Asymmetric Flow Field-Flow Fractionation (AF4) instrument integrated with a multi-angle laser light scattering (MALLS) instrument was used for size separation and characterization of the liposomes and nanogels (model DAWN EOS, Wyatt Technology, Santa Barbara, CA). A 250 μm spacer was used to define the flow channel thickness, and a MWCO regenerated cellulose membrane with a 10 kDa cutoff was used for the cross-flow partition. Tris-TAPS-NaCl buffer was used as the carrier solution in all AF4 runs, and the flow was controlled using vendor-supplied software (Eclipse 2, Wyatt Technology). For the control liposomes, 10 μL of the solution was injected at a flow rate of 0.2 μL/min, and the separation was conducted with a 1 mL/min channel flow with a crossflow that was linearly reduced from 0.8 mL/min to 0 mL/min over a period of 70 min. For the templated nanogels, the same conditions were used, except with a 30 μL sample injection volume and 60 min elution time. MALLS data were collected simultaneously at 10 scattering angles on the eluting sample.

The raw MALLS data (intensity vs. scattering angle) was analyzed as follows using the instrument software. From the Rayleigh-Debye-Gans Theory, the light scattering equation for non-interacting particles can be written as:

$$\frac{R(\theta)}{K^* c} = MP(\theta)[1 - 2A_2McP(\theta)] \tag{3.1}$$

where the form factor $P(\theta)$ is as follows:

$$P(\theta) = 1 - \frac{16\pi^2 n_0^2}{3\lambda_0^2}\sin^2\left(\frac{\theta}{2}\right)\left\langle R_g^2 \right\rangle + \ldots \tag{3.2}$$

Here, $R(\theta)$ is the excess Rayleigh ratio, K^* is a physical constant, c is the concentration, M is the molecular weight, A_2 is the second virial coefficient, n_0 is the index of refraction, λ_0 is the wavelength of the incident laser beam, and R_g is the radius of gyration. For dilute systems, the second virial coefficient A_2 can be neglected. Then, in the low concentration limit $c \rightarrow 0$, a plot of $\frac{R(\theta)}{K^* c}$ vs. $\sin^2\left(\frac{\theta}{2}\right)$ will be a straight line, and from the slope, the radius of gyration R_g can be obtained. The R_g for each eluting slice can thus be obtained, and these values can be combined to construct a particle size distribution[68,78].

Transmission Electron Microscopy (TEM). TEM of alginate nanogels was performed on a Philips EM 400T microscope operating at 120 kV equipped with a Soft Imaging System CCD camera (Cantega 2K). TEM samples were prepared by

dropping diluted dispersions of the nanogels onto 600-mesh carbon-coated copper grids, following which the grids were immediately freeze-dried (lyophilized).

Optical Microscopy. Optical micrographs of larger liposomes and alginate gel particles were obtained using a Carl Zeiss Axiovert 200 inverted microscope with a 40x differential interference contrast (DIC) objective.

3.3. RESULTS AND DISCUSSION

3.3.1. Nanogel Synthesis

The template liposomes used here are formed from a mixture of DPPC:cholesterol:DCP in a molar ratio of 7:2:1. The major component, DPPC, is a zwitterionic lipid having a T_m of ≈ 42 °C, which means the liposome bilayers are in their gel state at room temperature[42]. We incorporated cholesterol in our lipid formulation because low amounts of cholesterol further enhance membrane permeability near T_m (see below)[40,42]. DCP is an anionic lipid that gives a net negative charge to the bilayers, which in turn prevents aggregation of liposomes through electrostatic (double-layer) repulsions[40,42].

To prepare liposomes containing alginate, we first added 1 % w/v sodium alginate to Tris-TAPS-NaCl buffer and then injected the lipid formulation in IPA into this buffer solution. This procedure results in liposomes containing some sodium alginate in their cores (see below for further size characterization). We then subjected

the liposomes to five freeze-thaw cycles with liquid nitrogen and hot tap water. Freeze-thaw cycles are useful for enhancing encapsulation of solutes like alginate, since freezing tends to disrupt membrane bilayers, which may cause the solute to enter the liposome upon thawing and membrane reformation[79]. Unencapsulated alginate was thereafter removed via three centrifugation/buffer rinses, each at 13,200 rpm for 10 min, with resuspension in 1 mL Tris-TAPS-NaCl buffer. The last resuspension was done with 1 mL of Tris-TAPS-$CaCl_2$ buffer to initiate gelling of the sodium alginate chains in the liposomes via the divalent Ca^{2+} cations.

As discussed in the Introduction, we exploited the increased permeability of bilayers near their T_m to facilitate entry of Ca^{2+} into the liposome core[39,40,42,74]. To expose the sample to a temperature cycle across T_m, we placed alginate-containing liposomes in a heated water bath (60 °C) followed by an ice bath (0 °C), both under continuous stirring. The rate of temperature change was measured by a digital thermometer and was approximately 1 °C/s in both cases. Samples were exposed to 10 such temperature cycles across the T_m of DPPC. The net effect is that Ca^{2+} ions diffuse increasingly through the bilayer and crosslink the alginate chains, as shown in Figure 1. We are thus able to accomplish alginate gelation in the liposome cores using a low Ca^{2+} concentration gradient. The lipid bilayer still covers the gel particles, and so what we have at this stage are nanosized lipobeads. The lipobeads were rinsed three times by centrifugation (13,200 rpm for 10 min) using 1 mL of Tris-TAPS-NaCl that also contained 2 mmol/L of the Ca^{2+} chelator, EDTA.

Next, we converted the lipobeads to nanogels. The lipid bilayers around the lipobeads were removed by adding 30 mmol/L of OBG. OBG is a single-tailed detergent that is known to disrupt lipid bilayers because the detergent has a very different (cone-shaped) molecular geometry compared to conventional lipids (which are cylinder-shaped). The OBG treatment results in a stable dispersion of calcium alginate nanogels. The nanogels were rinsed by centrifugation (13,200 rpm for 10 min) and resuspended in 0.3 mL Tris-TAPS-NaCl buffer. Nanogel dispersions in buffer remained stable over the period of observation (several weeks). For comparison with the nanogels, we also ran two controls through the same above procedure, *viz.* empty DPPC:cholesterol:DCP liposomes and the same liposomes encapsulating ungelled alginate (in the latter case, the Ca^{2+} gelation step alone was omitted).

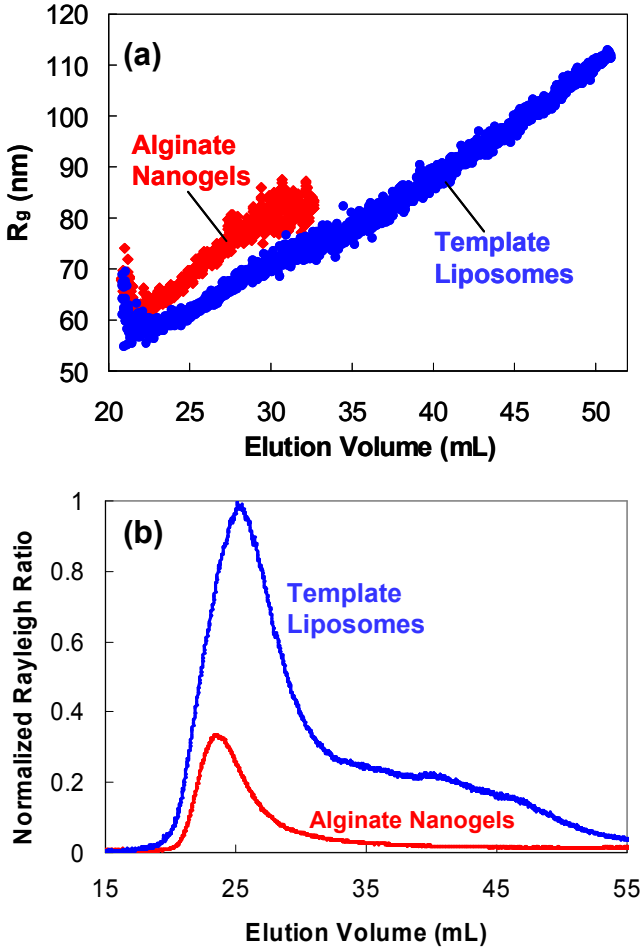

Figure 3.2. Data from light scattering for the template liposomes and alginate nanogels, following AF4 fractionation. The radius of gyration R_g is shown in (a) while the scattering intensity (normalized Rayleigh ratio) at 90° is shown in (b).

3.3.2. Nanogel Characterization by Light Scattering.

Figure 3.2 shows real-time light-scattering data for the template liposomes and for the alginate nanogels, following size-fractionation by AF4. As described in the Experimental Section, the light-scattering data for each AF4 elution slice are analyzed to obtain the corresponding radius of gyration R_g. Figure 3.2a plots the R_g as a function of elution volume while Figure 3.2b shows corresponding data for the scattered intensity (normalized excess Rayleigh ratio at 90°). The template liposomes

scatter strongly, and their R_g ranges from 55 nm to 112 nm. The nanogels prepared from these liposomes have a more narrow range of 65 nm to 85 nm for their R_g. Thus the nanogel sizes fall within those of the template liposome. Note that the peak scattered intensity in Figure 3.2b from the nanogels is about 4-fold weaker than that from the template liposomes, which means that the number density of nanogels is low compared to the liposomes.

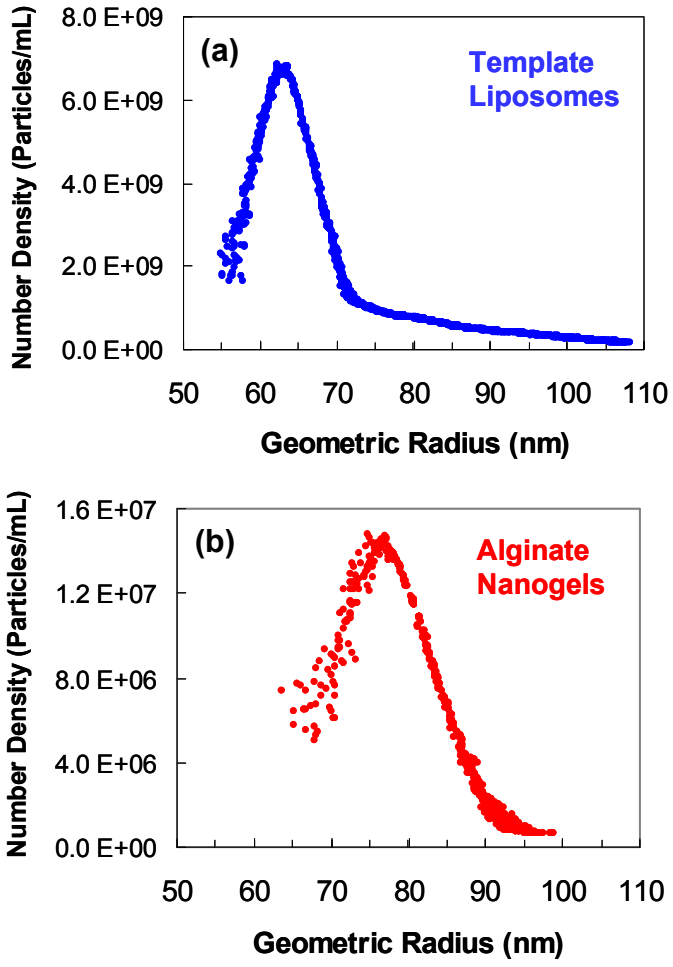

Figure 3.3. Size distributions of the template liposomes (a) and the alginate nanogels (b) obtained from the light scattering data in Figure 3.2.

The data in Figure 3.2 are converted into size distributions in Figure 3.3 for both the template liposomes and the alginate nanogels. The template liposomes (Figure 3.3a) have a size distribution peaked around a radius of about 63 nm followed by a long tail. The nanogels (Figure 3.3b) show a slightly wider peak centered around a radius of ca. 75 nm, but the long tail is absent. Thus, on average, the nanogels are slightly larger than the template liposomes, due in part to their tendency to swell in solution (see below). On the whole, however, the sizes of the two structures are quite comparable. In other words, the nanogels do correspond in size to their liposome molds, i.e., a true templating has been achieved. Note that the peak number density of the template liposomes is at least two orders of magnitude greater than that of the alginate nanogels. This is consistent with Figure 3.2b and implies that the yield of nanogels is quite low. We attribute the low yield to the low encapsulation efficiency of alginate in the liposomes. The encapsulation efficiency of polymers in liposomes is generally quite low (< 10 %), especially for large polymer coil sizes[80].

We further confirmed nanogel formation by comparing the nanogel sample to the two controls (empty liposomes; liposomes with ungelled alginate), following OBG detergent treatment. Figure 3.4 plots the scattered intensity (normalized excess Rayleigh ratio at 90°) for each of these samples as they elute from the AF4 device. The OBG should disrupt the liposomes in both controls and convert them into smaller micelles, which in turn should get removed by the centrifugation/buffer rinses. Thus, we expect to see minimal scattering from the control samples. On the other hand, the nanogels should remain intact upon OBG treatment, and the rinsed nanogel dispersion

should still scatter strongly. This is indeed what we find in Figure 3.4: the scattering from the nanogels is quite high, whereas the scattering from each of the two controls is negligible. Figure 3.4 thus confirms that we have indeed formed nanogel particles by our procedure.

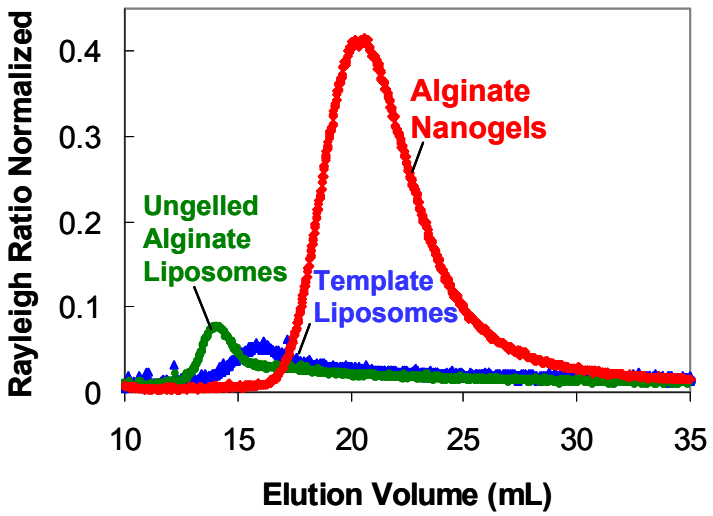

Figure 3.4. Light scattering intensities (normalized Rayleigh ratios) at 90° for samples passed through the AF4 setup following OBG detergent treatement. Data are shown for the template liposomes (blue), liposomes containing ungelled alginate (green), and alginate nanogels (red). Only the nanogels show a significant scattering intensity.

3.3.3. Nanogel Characterization by TEM

In addition to the indirect characterization by light scattering described above, we have also obtained direct images of nanogels using TEM. To obtain these images, drops of the rinsed nanogel dispersion were placed on TEM grids, which were then freeze-dried. No further contrast enhancement or staining was done. TEM images of freeze-dried alginate nanogels are presented in Figure 3.5, where on average we see

distinct spherical structures, well-separated from one another. The spheres have radii around 25-50 nm, which are smaller than the values measured by light scattering. However, the TEM sizes correspond to dried nanogels whereas the light scattering was done on nanogels in solution. Indeed, alginate nanogels in aqueous solution are known to swell up to several times their dehydrated size[27,81]. We also performed TEM studies on a control sample of freeze-dried template liposomes, but no structures could be observed (results not shown). This is consistent with the notion that liposomes are fragile, self-assembled structures that get disrupted during the freeze-drying process.

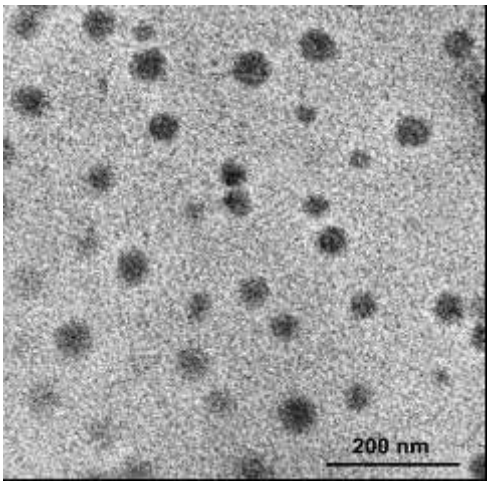

Figure 3.5. Typical TEM image of freeze-dried alginate nanogels. The nanogels are relatively monodisperse and exhibit the shape and size of their liposome templates.

3.3.4. Nanogel Response to Salt (NaCl)

The above data confirm the successful synthesis of alginate nanogels using liposomes as templates. But do these nanogels show the same responsive properties as much larger alginate gels? To test nanogel responsiveness, we have examined the

effect of adding NaCl to the nanogel dispersions. If Na^+ ions from the bulk solution were to exchange with the Ca^{2+} crosslinks in the alginate gel, the net degree of crosslinking of the gel would be lowered, and consequently the gel would swell more[27,81]. We have therefore monitored changes in the nanogel radius at increasing NaCl concentrations. The control sample of nanogels in Tris-TAPS-NaCl buffer corresponds to an overall NaCl concentration of 115 mmol/L. Additional NaCl was added to this sample to bring the Na^+ concentration to 250 mmol/L, and the sample was incubated overnight and then analyzed by light scattering. The same procedure was then repeated for an Na^+ concentration of 400 mmol/L. Figure 3.6 shows results for the radius of gyration R_g of the nanogels estimated from the light scattering data. As expected, we find a significant increase in nanogel radius with increasing NaCl concentration. These results demonstrate that nanogel properties can indeed be manipulated by tuning external variables such as the salt concentration.

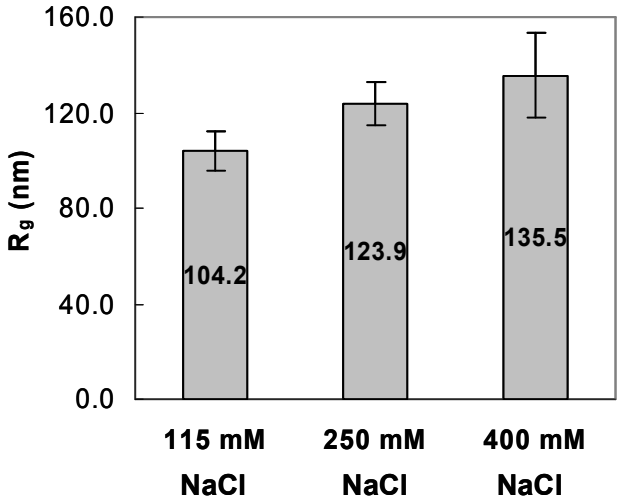

Figure 3.6. Sizes of alginate nanogels at different concentrations of NaCl. The data show an increase in size with increasing salt concentration.

3.3.5. Larger Gel Particle Synthesis

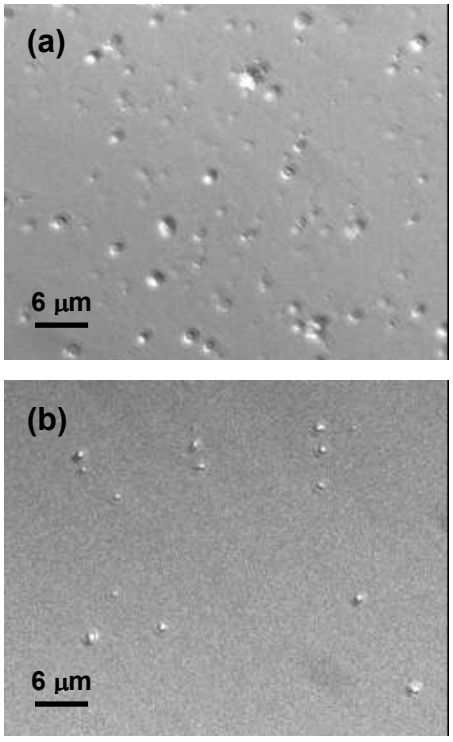

Figure 3.7. Optical (DIC) micrographs of alginate gels templated by larger (micron-sized) vesicles. (a) Before OBG treatment (i.e., with lipid shell intact), and (b) after OBG treatment (i.e., bare gel particles).

All the results thus far have been for nanogels templated from relatively small liposomes (~ 100 nm in radius). A final question we address is whether we can control the size of the gels by varying the size of the template liposomes. By using a lipid formulation of DPPC:DCP (9:1 molar ratio), we can obtain liposomes of ca. 400 nm to 500 nm in radius using the solvent injection method. Note that, at these larger sizes, the liposomes could well be a combination of unilamellar and multilamellar structures. Nevertheless, we have been able to encapsulate alginate in these liposome cores, and we have subsequently crosslinked the alginate chains by exposure to a Ca^{2+} gradient to yield micron-sized gel particles. Evidence for gel formation in this case

can be obtained directly from optical (DIC) microscopy. Figure 3.7a shows a micrograph of the gel particles with intact lipid bilayers (before OBG treatment). We can resolve a large number of distinct spherical structures in this image. Figure 3.7b shows the same sample after treatment with 30 mmol/L OBG. Here again, we find distinct gel particles with approximately the same size as in Figure 3.7a, although the number density of such particles is significantly lower. For comparison, we also obtained DIC micrographs of a control sample of liposomes alone – in this case, upon exposure to OBG, the liposomes were destroyed, and no structures could be resolved by DIC. Light scattering also confirmed that the average radius of the gel particles was around 500 nm; i.e., comparable to that of the template liposomes. The data suggest that our templating strategy can be generalized to gels over a range of sizes.

3.4. CONCLUSIONS

We have used liposomes to template relatively monodisperse populations of alginate nanogels. The solvent-injection method was used to form the liposomes and simultaneously encapsulate sodium alginate in the liposome cores. Alginate gelation in the liposome cores was accomplished using a low Ca^{2+} concentration gradient by exploiting the increased transbilayer permeability near T_m. The lipid coating around the nanogels was then removed by the addition of OBG detergent. Light scattering and TEM confirmed the formation of nanogels. Experiments with two different liposome sizes showed that the gel particles conform to the sizes of the templates. The nanogels described here could be useful for biomolecule encapsulation either in controlled release experiments or for single molecule fluorescence studies.

4. MICROFLUIDIC DIRECTED ASSEMBLY OF ALGINATE NANOGELS

4.1. INTRODUCTION

Following the results of the bulk experiments to template alginate nanogels in Chapter 3, we sought to improve size control of the nanogels by replacing the bulk solvent-injection method with the microfluidic approach described in Section 2.4. As mentioned earlier, the microfluidic approach gives better control over liposome sizes and encapsulation[55]. In this approach, a lipid/solvent stream is hydrodynamically focused by an aqueous buffer solution that is miscible with the solvent. The liposomes form at the interface between the two streams, where the solubility of lipid decreases as the aqueous buffer diffuses into the solvent containing the lipid. The liposome size can be controlled by varying the volumetric flow-rate-ratio (VFRR) of the aqueous buffer outer streams to the central focused lipid-solvent stream[82].

The adaptation of this method for the assembly of alginate nanogels is shown in Figure 4.1. It involves on-chip formation of liposomes and simultaneous encapsulation of sodium alginate. After the samples are collected at the microchannel outlet, the ionic crosslinking of the liposome cores into nanogels can then be conducted off-chip. Note that, while the ultimate goal would be the complete on-chip synthesis of nanogels, the approach outlined here would be a step towards that goal.

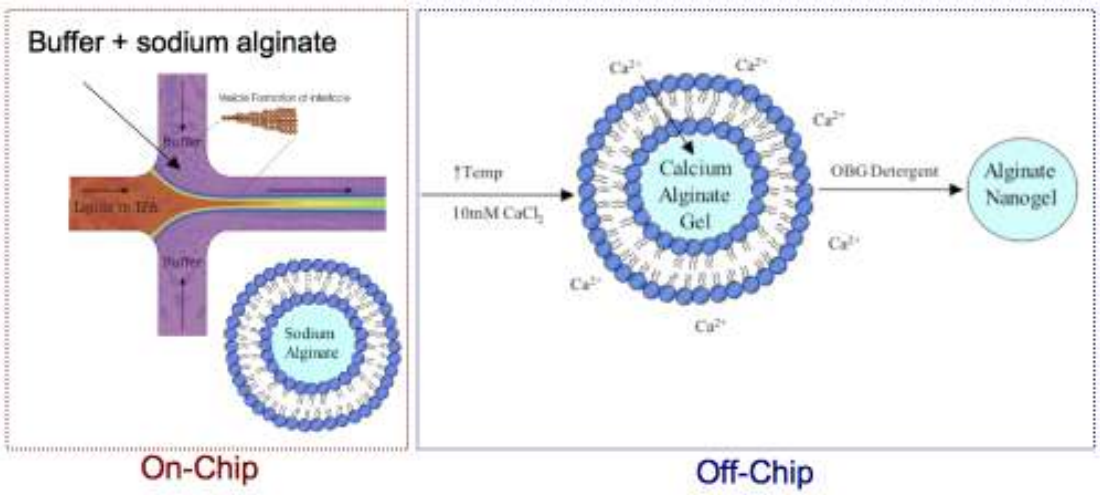

Figure 4.1. Microfluidic approach to the directed assembly of alginate nanogels. On-chip steps of liposome self-assembly and simultaneous encapsulation of sodium alginate are followed by off-chip purification, temperature-triggered liposome permeabilization, ionic crosslinking via Ca^{2+}, and subsequent lipid removal.

The studies in this Chapter primarily concern the on-chip part, i.e., formation of liposomes with encapsulated sodium alginate. We encountered some challenges in these studies, including phase separation at the microfluidic mixing interface due to poor polymer-solvent interactions between the alginate-buffer streams and the focused lipid-solvent stream. Ultimately we were able to solve some of these issues and produce liposomes in the microfluidic device, but the encapsulation of sodium alginate in these liposomes was quite low. The off-chip steps were not carried out due to the low encapsulation of the hydrogel precursor molecules, and we concluded that the encapsulation would be improved with an alginate oligosaccharide or a monomeric hydrogel precursor, both of which would diffuse quickly in the microfluidic mixing region and also interact less with the solvent, and thus increase the amount encapsulated by the liposomes upon assembly in the device.

4.2. EXPERIMENTAL SECTION

Materials. Alginic acid sodium salts (20 cP and 250 cP), fluoresceinamine isomer I (FA), N-Hydroxysulfosuccinimide sodium salt (NHS), N-(3-Dimethylaminopropyl)-N′-ethylcarbodiimide hydrochloride (EDC), dihexadecyl phosphate (DCP), and sodium azide (NaN_3) were obtained from Sigma Aldrich. Buffer components Tris free base was purchased from Amresco, and N-tris(hydroxymethyl)methyl-3-amino-propanesulfonic acid (TAPS) was obtained from Midwest Scientific. Sterile luer-lock plastic syringes (1 mL and 3 mL) were obtained from Daigger. Lipophilic tracer 1,1'-dioctadecyl-3,3,3',3'-tetramethylindodicarbocyanine perchlorate (DiD) was obtained from Invitrogen (structure in Figure 4.2).

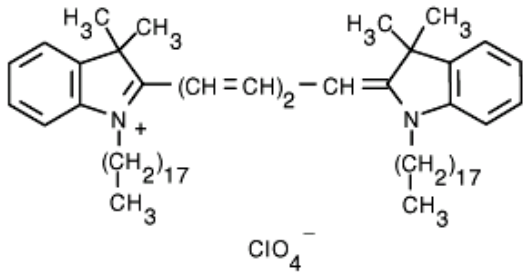

Figure 4.2. Chemical structure of DiD intercalating membrane dye (Invitrogen).

1,2-dipalmitoyl-*sn*-glycero-3-phosphocholine **(**DPPC) and cholesterol were obtained from Avanti Polar Lipids. Tris-TAPS-NaCl buffer (pH 8.0) was prepared by combining 50 mM Tris, 50 mM TAPS, and 15 mM NaCl. 3 mM NaN_3 was added to all buffer solutions to prevent bacterial growth. This buffer was used for all sample preparation and characterization techniques. The primary lipid formulation consisted of DPPC:cholesterol:DCP (7:2:1 molar ratio) and 1.0 mol% DiD lipophilic tracer.

Microfluidic Device Fabrication. Microfluidic devices were fabricated in silicon and bonded to borosilicate glass using standard microfabrication processes. A thin film of positive tone photoresist was spin-coated onto the front side of a double side polished silicon substrate wafer with a thickness of ≈ 290 μm. Networks of fluidic channels with widths of ≈ 21 μm were patterned in the photoresist using contact photolithography. Device patterns were transferred into the substrate using Bosch Process deep reactive ion etching to a depth of ≈ 39 μm.

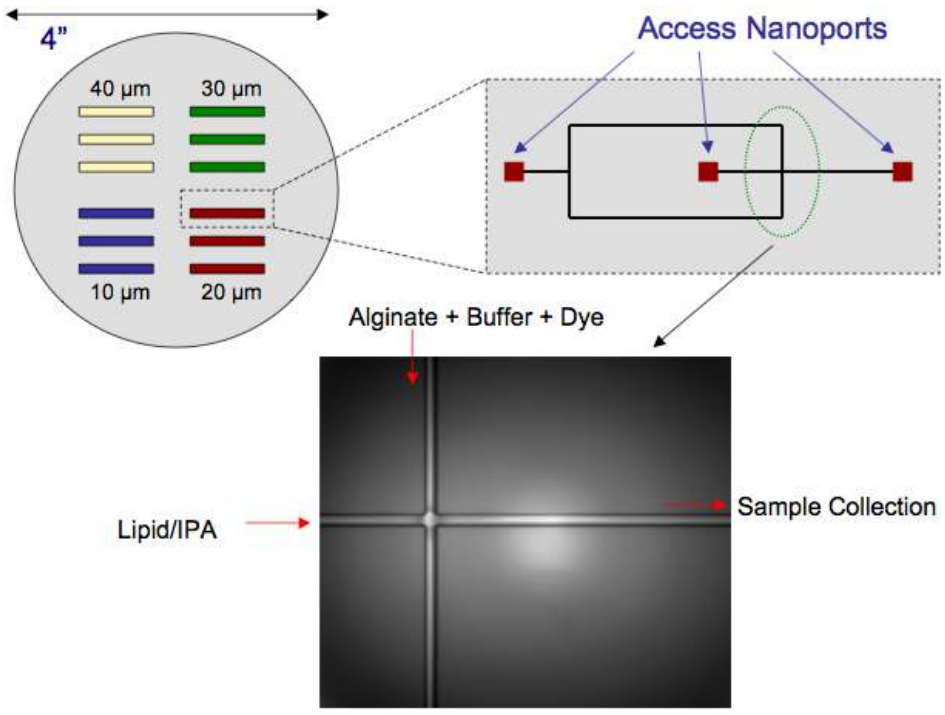

Figure 4.3. Schematic of microfluidic device design with an enlarged illustration of the hydrodynamic focusing device. With the small channel dimensions required for microfluidic experiments, multiple devices of different channel widths can be fabricated onto a single 4 in. wafer.

Microfluidic Liposome Formation. Liposomes encapsulating sodium alginate were self-assembled with controlled microfluidic mixing by hydrodynamic focusing[82]. The lipid film was redissolved in dry 0.1 μm-filtered solvent to obtain a 6.25 mM solution. The lipid solution and the alginate in Tris-TAPS-NaCl solution were each loaded in a plastic 3 mL luer lock syringe and were connected to the device access nanoports, as shown in Figure 4.3. Syringe pumps were used to control the flow of lipid-solvent solution into the center channel and alginate in buffer into the side channels to hydrodynamically focus the central lipid-solvent stream.

Microfluidic synthesis was monitored with an inverted optical microscope used in epifluorescence mode. Imaging was done through the cover wafer with plan apochromat air immersion objectives of 20x and 40×, and numerical aperture 0.95. A metal halide arc lamp was used with a 625 to 655 nm band pass filter for fluorescence excitation of DiD, and fluorescence emission was isolated with a 660 nm dichroic mirror and refined with a 665 to 715 nm band pass filter. For detection of the FA dye, a 450 to 490 nm band pass filter was used, and the fluorescence emission was isolated with a 515 to 565 nm band pass filter. These dyes were selected such that the emission spectrum of the FA dye would be isolated from the excitation range of the DiD. Images were acquired with an electron multiplying device camera.

AF4-MALLS. The Eclipse AF4 / Dawn EOS MALLS used in Chapter 3 was also employed here. 20 μL of each sample collected from the microfluidic formation were loaded into the AF4 injection loop, and fractionation was conducted with a 1 $mLmin^{-1}$

channel flow and a 2.0 mL min^{-1} to 0.0 mL min^{-1} linearly decreasing crossflow gradient over 75 min. MALLS data was collected on eluting samples at 10 angles simultaneously. A coated sphere model[83] was applied to the data using an estimated bilayer thickness of 5 nm to determine geometric radii distributions of the liposomes.

4.3. Results and Discussion

4.3.1. Fluorescent Labeling of Sodium Alginate

To visually observe the microfluidic focusing interface, sodium alginate was labeled by adapting a previously reported method[84]. 1.78 % w/v aqueous solutions of 250 cP and 20 cP sodium alginate were incubated with 9 mM EDC and 9 mM NHS for 2.5 h, and 1 mM FA was added to the solution and was incubated for another 20 h. The sample was dialyzed against Tris-TAPS-NaCl for 24 h, with three buffer exchanges. The resultant fluorescently-labeled 20 cP and 250 cP alginate samples are shown in Figure 4.4a and Figure 4.4b, respectively.

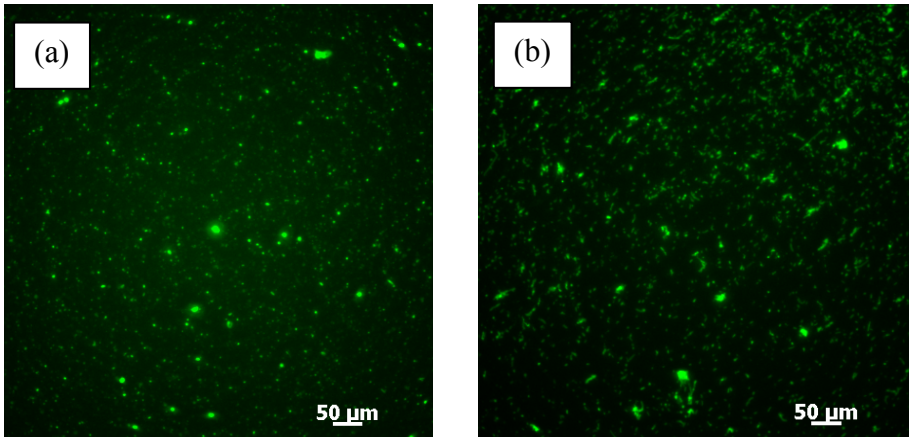

Figure 4.4. Fluorescence micrographs of 1.78% w/v of (a) 20cP and (b) 250 cP sodium alginate tagged with fluoresceinamine (FA) dye in Tris-TAPS-NaCl buffer.

4.3.2. Microfluidic Formation of Alginate-Encapsulating Liposomes

Initially, we dissolved the lipid in IPA and used a solution of 1% w/v of the 250 cP sodium alginate in aqueous buffer. At the continuous interface between the center lipid-IPA and sheath alginate-buffer streams in the microfluidic device, unfavorable polymer-solvent interactions occurred, which had a pronounced negative effect on the formation of liposomes. Phase separation was observed immediately after the onset of flow (Figure 4.5a) and became progressively worse after 15 min (Figure 4.5b). Shortly thereafter this phase separation completely obstructed fluid flow in the microfluidic channel at the hydrodynamic focusing interface, preventing the collection of sample.

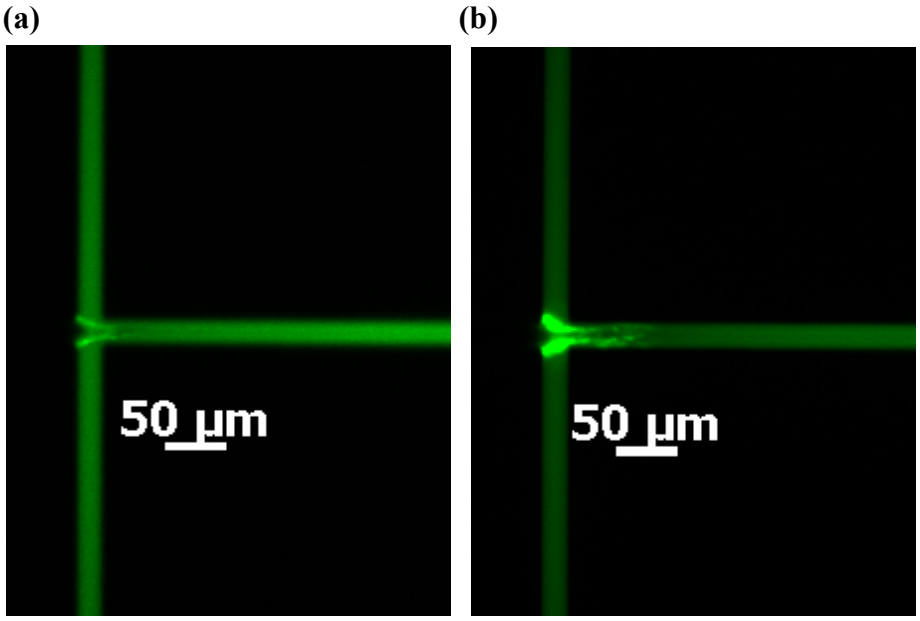

Figure 4.5. Chemical insolubility between the 250 cP sodium alginate polymer and 100% IPA after (a) 1 min and (b) 15 min of flow initiation.

To improve the chemical compatibility between the mixing streams, we made modifications to the lipid and alginate formulations. In the bulk solvent-injection method (Chapter 3), the lipid is dissolved in a much smaller volume of IPA and is injected once into a much larger volume of the buffer solution – thus any phase separation between the two solutions was transient. The microfluidic method requires a continuous interface between the solvent and aqueous streams, with a higher surface-to-volume exposure of the polymer to the solvent, which magnified the chemical incompatibilities. We experimented with various solvent concentrations, lipid concentrations and alginate concentrations, as well as with the lower viscosity (20 cP) sodium alginate polymer, and were finally able to resolve working formulations for the lipid and sodium alginate.

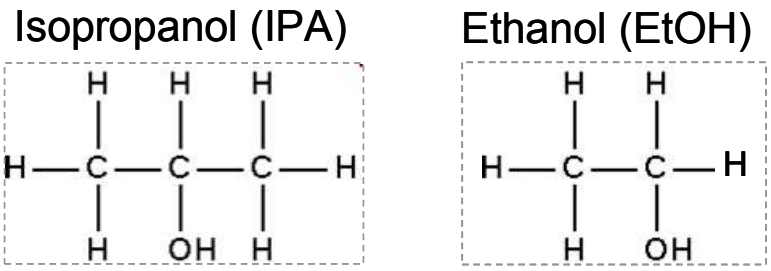

Figure 4.6. Chemical structures of isopropanol (IPA) and ethanol (EtOH). EtOH is slight less hydrophobic than IPA, which cause less phase separation of the alginate a the hydrodynamic focusing interface of the microfluidic channel.

The working lipid formulation was a 6.25 mM concentration of lipid in 3.2 mL of a solvent mixture consisting of 75% ethanol (EtOH): 25% IPA by volume. The lipid was dissolved in 0.8 mL of IPA first, and then three 0.8 mL aliquots of EtOH were added. EtOH was chosen due to its similarity to IPA, but its slightly more hydrophilic chemical structure due to one less methylene group than IPA (Figure 4.6)

improved the solvent compatibility with the sodium alginate compared to the initial 100% IPA solvent. The lipid solubility was maintained in the 75% EtOH: 25% IPA mixture, while decreasing the adverse interactions with sodium alginate during the microfluidic-directed formation. The working sodium alginate formulation was a 0.25% w/v 20 cP sodium alginate solution in Tris-TAPS-NaCl. A decrease in concentration and a move to a lower viscosity alginate helped mitigate the poor polymer-solvent interactions at the mixing interface.

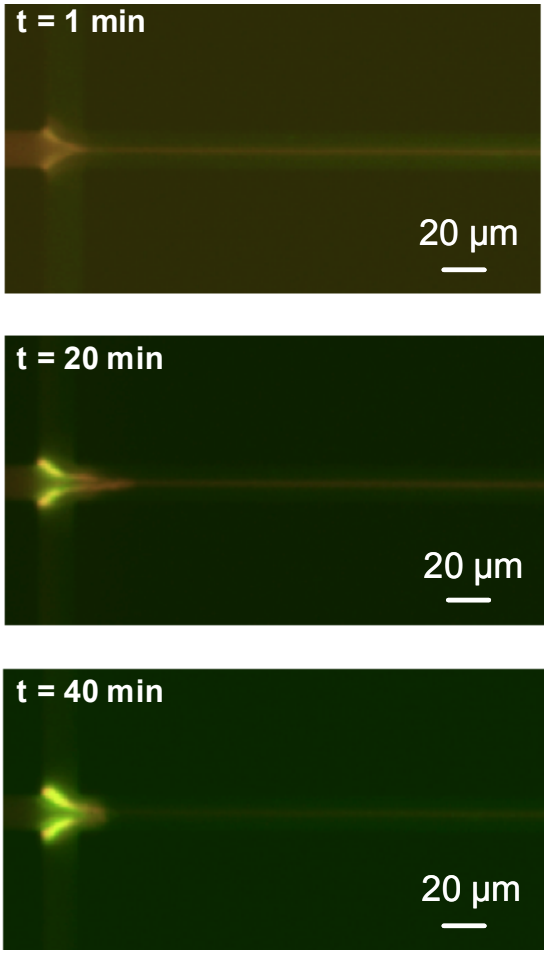

Figure 4.7. Microfluidic formation of alginate-containing liposomes. The images with dual channel acquisition show the DiD-labeled lipid (red) and FA-labeled alginate (green). Over the course of the experiment, interfacial build-up due to phase separation of alginate in the hydrodynamic focusing region increased near the glass surface, but did not prevent the continuous formation of liposomes.

Fluorescence micrographs of the microfluidic directed assembly of liposomes based on this formulation over time are shown in Figure 4.7. Although phase separation increased at the mixing interface over the duration of the experimental run, the microchannel was never completely obstructed and we were able to collect liposomes at volumetric flow-rate-ratios (VFRRs) of 6:1, 9:1, and 12:1.

4.3.3. Size Characterization with AF4-MALLS

Liposomes collected from the microfluidic device outlet at each VFRR were characterized by AF4-MALLS, and their size distributions are shown in Figure 4.8a. Each data point represents a MALLS measurement made on an AF4 size-fractionated component of the entire liposome sample[68]. Figure 4.8b shows a plot of the average radius and the standard variability of each sample as calculated by one standard deviation from the mean. Average radii were weighted by the particle densities from Figure 4.8a to give a more representative average value for each population. The data indicate that we produced relatively monodisperse and discrete nanoscale liposome populations. The expected trends of smaller liposome size and narrower size distribution with increasing VFRR are seen in Figure 4.8b[22]. Figure 4.8b displays a nearly linear correlation between average radius and VFRR. The microfluidic method thus leads to improved size control of alginate-containing liposomes over those formed by the bulk method in Chapter 3, while also having the advantage of fewer processing steps. The sizes of these liposomes are within a relevant range for therapeutic applications, and in general are smaller than the alginate nanogels synthesized in Chapter 3.

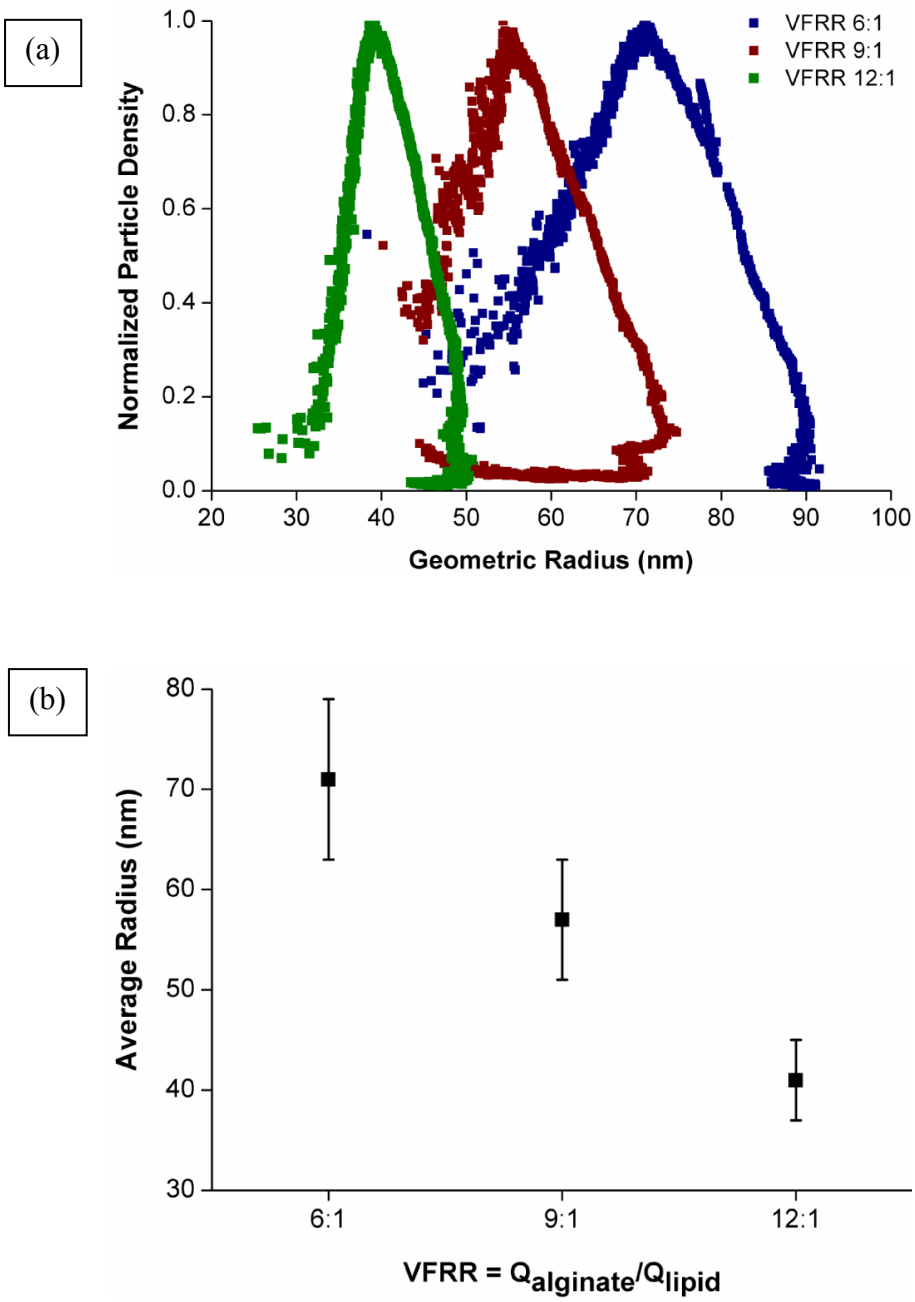

Figure 4.8. Size characterization of liposomes encapsulating sodium alginate. (a) Size distributions of liposomes with 20 cP sodium alginate, synthesized at varying VFRRs and (b) the average radius and variance of each of the above distributions. Both sets of data show the expected trend of decreasing size and narrowing size distribution with increasing VFRR.

4.3.4. Encapsulation of Sodium Alginate

Dual-channel fluorescence micrographs of a 1:50 diluted sample of alginate-containing liposomes following microfluidic formation at a 6:1 VFRR are shown in Figure 4.9. An overlay of the DiD-labeled liposomes (red) and the FA-labeled alginate (green) was used to qualitatively confirm encapsulation before proceeding. The incidence of liposomes with overlapped fluorescence of alginate molecules was extremely low . In the case of the 9:1 and 12:1 VFRR samples, the encapsulation was practically negligible (data not shown). This is probably because the liposomes become smaller as the VFRR increases (Figure 4.8), making the encapsulation of the alginate, a relatively large macromolecule[85], less likely.

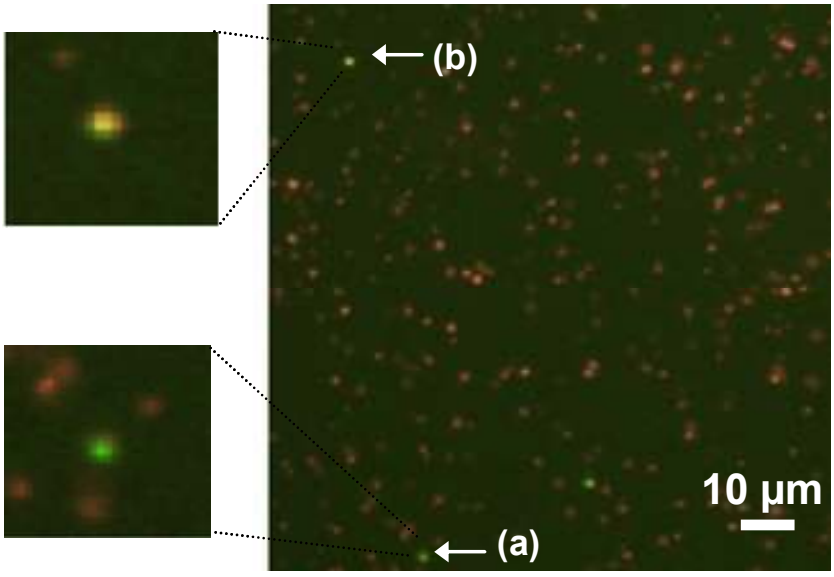

Figure 4.9. Dual-channel fluorescence micrographs of liposomes encapsulating 20 cP sodium alginate, formed at a VFRR of 6:1. The red and (a) green particles indicate empty liposomes and unencapsulated alginate, respectively. The (b) yellow particle is a result of overlapping red and green fluorescence, which is an indication of a liposome encapsulating sodium alginate. The low incidence of yellow particles indicates that the encapsulation efficiency was extremely low.

Our results suggest that the microfluidic method may be better suited for forming liposomes that encapsulate lower molecular weight precursors and thereafter for templating the assembly of nanogels from those precursors. Further modifications to our current approach would likely aid in increasing the encapsulation efficiency of sodium alginate. One such modification might be to cleave the alginate into smaller oligosaccharides via enzymatic digestion. Smaller oligosaccharides would likely be more compatible within the microfludic mixing interface, which would allow us to use a more concentrated alginate formulation and thus increase the potential for encapsulation within the liposomes.

4.4. CONCLUSIONS

We have explored a microfluidic approach for the assembly of liposomes encapsulating sodium alginate, which is a necessary step towards the goal of forming alginate nanogels using microfluidics. Formulations of lipid and sodium alginate solutions were modified to enable assembly of nanoscale liposomes containing alginate by microfluidic hydrodynamic focusing. The average size of the resultant liposomes could be altered by changing the flow rates of the lipid and alginate streams. The extent of encapsulation of the alginate proved to be quite low, which was attributed to the large size of the polymer relative to the sizes of the liposomes. We believe our method would be more suitable for the templating of low molecular weight precursors, such as oligomers or monomers, and this will be investigated further in Chapter 5.

5. MICROFLUIDIC DIRECTED ASSEMBLY OF LIPID-HYDROGEL HYBRID NANOPARTICLES*

*The results in this chapter are currently in preparation for a manuscript submission to Langmuir **(2009)**.

5.1. INTRODUCTION

Soft nanoparticles such as nanoscale lipid vesicles, hydrogel nanoparticles, and hybrids of the two have many important applications in healthcare and the life sciences[8,86]. Such nanoparticles have been applied in areas of single molecule manipulation and metrology[87], sensors[88], biomedical imaging[89], and chromatography[15]. Particular interest has grown in these nanoparticles as potential carriers for the targeted delivery and controlled release of therapeutic agents for diagnostic and treatment purposes[5,11,18,21,90]. Although many types of these nanoparticles have been developed, few have advanced to clinical use because of a lack of consistent toxicology data, which in turn arises partly because nanoparticle preparation techniques yield erratic results across laboratories[91].

Nanoparticles are largely synthesized using bulk techniques. Phospholipid-based nanoparticles are typically synthesized using evaporation-rehydration or solvent-injection methods, while polymeric nanoparticles are traditionally prepared using emulsion-based or solvent-evaporation methods[92-94]. The technical limitations associated with bulk methods for synthesizing soft matter nanoparticles constitute a significant impediment to the realization of many of these applications. These

limitations include nanoparticle size distributions that are polydisperse, irreproducible from batch to batch, and strongly dependent on chemical formulation[18,95]. A root cause of these problems is the disparity between macroscopic control over the reaction of nanoparticle precursor solutions and the microscopic fluid environment which determines the formation of nanoparticles. These limitations often necessitate the use of post-processing techniques such as high frequency sonication, freeze-thaw cycling, or membrane-extrusion to homogenize nanoparticle size and composition, which can decrease yield, increase assembly time, and can be incompatible with biological applications[15].

To address these limitations, a variety of microfluidic methods have recently been developed to synthesize soft nanoparticles with improved control over size distribution, as size has been determined to be a critical factor in influencing nanoparticle efficacy or toxicity for a particular application[91,96]. One such method is the use of microfluidic hydrodynamic focusing[52] to precisely control the convective-diffusive mixing of miscible liquids at the nanometer length scales and microsecond time scales that determine the formation of nanoparticles. This approach has been used to direct the self-assembly of lipid molecules into nanoscale lipid vesicles of controlled size in a continuous and reproducible manner[55], obviating the need for post-processing to homogenize nanoparticle size. Similar microfluidic approaches have been used to produce polymeric nanoparticles[18,19].

Beyond these single-material lipid or polymer nanoparticle systems that have been synthesized using microfluidic devices, relatively few microfluidic methods for the precisely controlled synthesis of multiple-material hybrid nanoparticle systems have been demonstrated even though there are many known important applications for them. In particular, lipid-hydrogel hybrid nanoparticles, also known as lipobeads, combine many of the advantageous material properties of the individual constituents for therapeutic applications[8,12]. The hydrogel interior improves both the mechanical stability of hybrid lipid-hydrogel nanoparticles and the controlled release of encapsulated therapeutic agents, while the many useful surface properties of the exterior lipid vesicle are retained for both stealth capability and targeted delivery[13,16,70,93,98,99]. This potential therapeutic utility motivates the development of advanced microfluidic methods to control the synthesis of these more structurally complex soft matter nanostructures.

In this Chapter, we present a microfluidic approach to the directed assembly of monodisperse lipid-hydrogel hybrid nanoparticles of controlled size. We selected poly(N-isopropylacrylamide) (PNIPA) as our model polymer, as it is one of the most widely studied thermo-responsive polymers for therapeutic applications, and also because it has been used recently for the bulk formation of lipobeads[14,44,72,73]. As shown in Figure 5.1, our approach utilizes microfluidic hydrodynamic focusing to control the convective-diffusive mixing of two miscible liquids[82] that separately contain the precursors to our hybrid nanoparticles. One solution contains a mixture of phospholipids and cholesterol in isopropanol (IPA) and forms the central stream in

Figure 5.1a. The outer sheath flow consists of an aqueous solution of N-isopropyl-acrylamide (NIPA), crosslinker, and free-radical initiator, in phosphate-buffered saline (PBS).

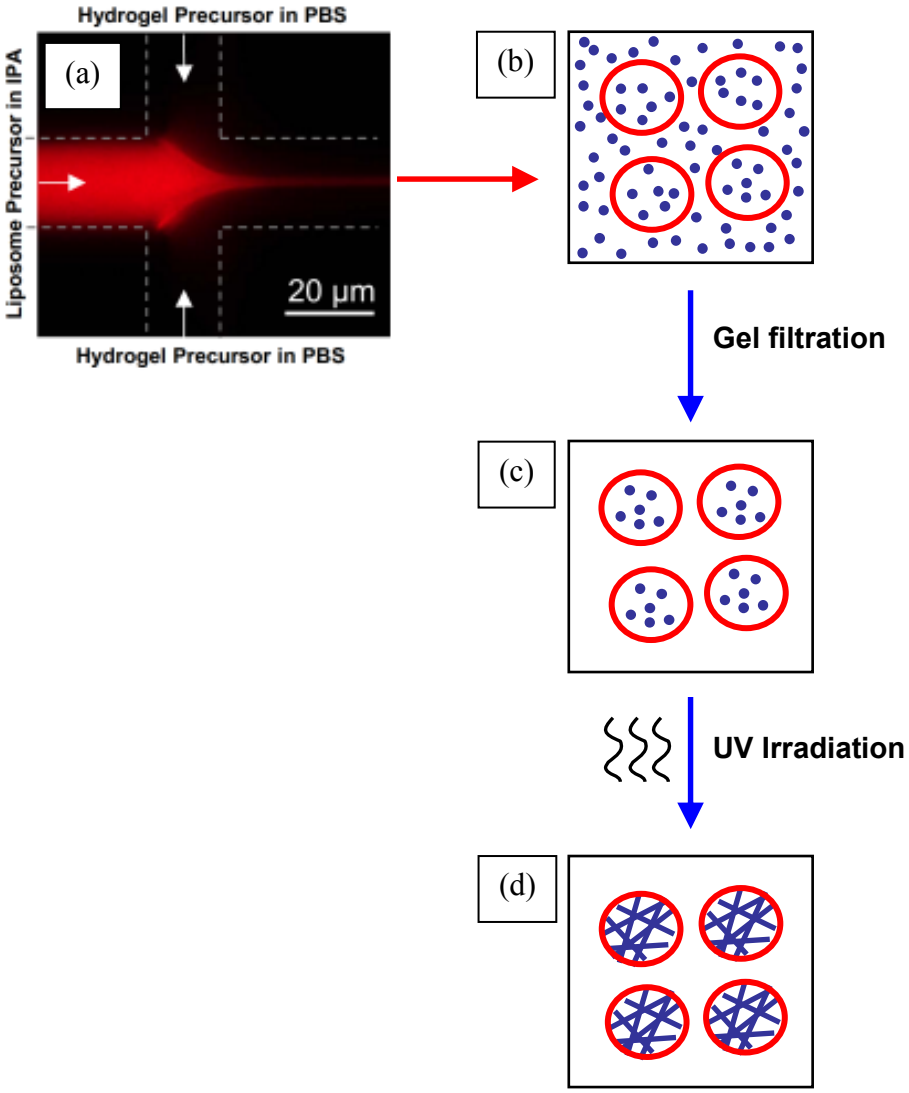

Figure 5.1. Schematic of the on-chip microfluidic-directed assembly and off-chip polymerization of lipid-PNIPA hydrogel nanoparticles. (a) A solution of lipid and lipophilic tracer DiD (red) dissolved in IPA was hydrodynamically focused by a solution of the hydrogel precursor in buffer. Microfluidic mixing was used to direct the formation of nanoscale lipid vesicles with encapsulated gel precursors, and the sample was collected (b) at the device outlet. (c) The extravesicular gel precursor material was removed by gel filtration, and the particles were resuspended in buffer. (d) Subsequent UV irradiation initiated the free-radical polymerization of the liposome interior which produced lipid-PNIPA hydrogel nanoparticles.

Using this approach, we can direct the assembly of liposomes at the interface between the two streams, and these liposomes will encapsulate the contents of the aqueous solution, i.e., the hydrogel precursors. Moreover, by varying the volumetric flow-rate-ratio (VFRR) of the aqueous outer streams to the central lipid-IPA stream, the convective-diffusive mixing conditions at the interface are altered, and thereby the size of the liposomes can be controlled[82]. The liposomes at the outlet of the microfluidic chip are then collected, purified by gel filtration, and UV-irradiated off-chip to polymerize the encapsulated precursors into a hydrogel core. Hybrid nanoparticles of controlled size can thus be prepared in the 150 to 300 nm diameter range. The above approach can be extended to the assembly of other hybrid nanoparticle systems of interest[45]. Microfluidic assembly may offer greater control over nanoparticle size and compositional requirements, as well as provide a systematic platform for nanoparticle characterization.

5.2. EXPERIMENTAL SECTION

Materials.[100] The lipid dye 1,1'-dioctadecyl-3,3,3',3'-tetramethylindodicarbocyanine perchlorate (DiD) was obtained from Molecular Probes, and 1,2-dipalmitoyl-*sn*-glycero-3-phosphocholine (DPPC) and cholesterol from Avanti Polar Lipids. Dihexadecyl phosphate (DCP), N-isopropylacrylamide (NIPA) (97% purity), N,N'-methylenebis(acrylamide) (MBA) (99% purity), 2,2-diethoxyacetophenone (DEAP), octyl-β-D-glucopyranoside (OBG), phosphate buffered saline (PBS) pH 7.4, and sodium azide (NaN_3) were obtained from Sigma-Aldrich. Polydimethylsiloxane

(PDMS) (Sylgard 184) was purchased from Dow Corning. Hamilton gas-tight glass syringes and anotop syringe filters were obtained from Fisher Scientific. D-Salt columns and Slide-A-Lyzer dialysis cassettes were purchased from Pierce.

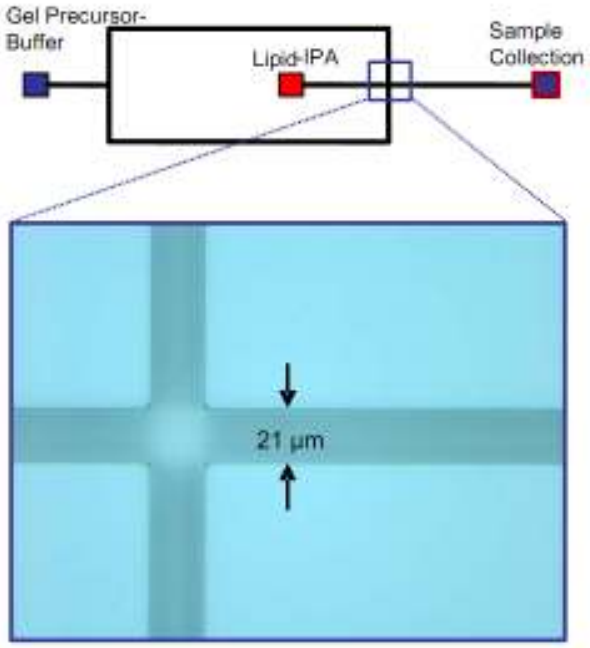

Figure 5.2. Device schematic and optical micrograph of the microfluidic hydrodynamic focusing cross junction. Microchannels were fabricated in a silicon substrate which was anodically bonded to a borosilicate glass cover. The microfluidic channel was 21±1 µm wide and 39±1 µm deep.

Microfluidic Device Fabrication. A schematic and brightfield micrograph of the microfluidic device is shown in Figure 5.2. Microfluidic devices were constructed using standard microfabrication processes. A thin film of positive tone photoresist was spin-coated onto the front side of a double-side-polished silicon substrate wafer with a thickness of ~ 290 µm. Networks of fluidic channels with widths of (21±1) µm (mean ± expanded uncertainty) were patterned in the photoresist using contact photolithography. Device patterns were transferred into the substrate using Bosch

Process deep reactive ion etching to a depth of (39±1) μm (mean ± expanded uncertainty). A thin film of silicon dioxide was deposited as an etch stop on the front side of the substrate using plasma enhanced chemical vapor deposition. A thin film of positive tone photoresist was spin-coated onto the back side of the substrate and a second layer of contact photolithography was used to pattern access holes aligned to the channel inlets and outlets. Access holes were then formed by deep reactive ion etching of the substrate through to the etch stop. The substrate wafer was immersed in buffered hydrofluoric acid to remove the silicon dioxide etch stop and finally cleaned with a mixture of ammonium hydroxide:hydrogen peroxide:water (~ 5:1:1 volume ratio) at a temperature of ~ 80 °C. A borosilicate glass cover wafer with a thickness of ~ 170 μm was anodically bonded to the front side of the substrate wafer to form enclosed microfluidic channels. Fluidic connectors were adhered to the back side of the substrate wafer to couple polyetheretherketone capillaries to the inlets and outlets of the microfluidic devices. The opposing end of each inlet capillary was attached to a gastight glass Hamilton syringe filled with reagent. The syringes were mounted onto syringe pumps (Harvard Apparatus) to control continuous fluid flow into the microchannels.

Epifluorescence Microscopy. An inverted optical microscope was used in epifluorescence mode to observe microfluidic formation of nanostructures. Imaging was done through the cover wafer with a plan apochromat air immersion objective of magnification 40× and numerical aperture 0.95. A metal halide arc lamp was used with a 625 to 655 nm band pass filter for fluorescence excitation, and fluorescence

emission was isolated with a 660 nm dichroic mirror and refined with a 665 to 715 nm band pass filter. Videos and images were acquired with either an electron multiplying or color charge coupled device camera. Following nanoparticle synthesis experiments, hybrid nanoparticles were suspended on a glass coverslip with a thickness of ~170 μm for inspection using the same optical setup.

Buffer Preparation. 0.01 M Phosphate buffered saline (PBS) (0.138 M NaCl, 2.7 mM KCl, pH 7.4) was used in all experiments unless otherwise specified. PBS was prepared in 18.2 MΩ filtered deionized water with the addition of 3 mM NaN_3 to prevent bacterial growth. All PBS solutions were filtered through a 0.1 μm syringe filter prior to use in sample preparation.

Lipid and Hydrogel Precursor Solutions. A mixture of DPPC:cholesterol:DCP (7:2:1 molar ratio) and 0.5 mol% DiD lipophilic tracer was used in the formation of the empty liposomes and lipid-hydrogel hybrid nanoparticles. The mixture was dissolved in chloroform in a glass scintillation vial and was dried down under dry nitrogen for 45 min to produce a thin lipid film, and the dried film was placed in a vacuum dessicator overnight to remove any residual solvent. The NIPA:MBA:DEAP (3.5%:0.35%:0.1% w/v) gel precursor solution was prepared in PBS. An Omnicure S2000 (EXFO Life Sciences, Canada) lamp (λ = 365 nm; 40 W cm^{-2}) was used to initiate free-radical polymerization of the bulk hydrogel precursor material. The onset of polymerization was observed immediately upon UV irradiation, and complete bulk gel formation was verified after 15 min of irradiation.

Precursors to Hybrid Nanoparticles by Microfluidic Flow Focusing. Nanoscale liposomes containing hydrogel precursors were synthesized using controlled microfluidic mixing by hydrodynamic focusing[82]. The lipid film was redissolved in dry 0.1 μm filtered IPA to obtain a 6.25 mM solution. The lipid solution and either the gel precursor (experimental) or PBS (control) solution were each loaded in a glass syringe and connected to the device inlets, as shown in Figure 5.2. Syringe pumps were used to control the flow of lipid-IPA solution into the center channel and PBS or gel precursor solution into the side channels to hydrodynamically focus the lipid-IPA stream, shown in Figure 5.1a. Empty liposomes were formed in PBS at VFRRs of 10:1, 15:1, 20:1, and 25:1, while liposomes encapsulating the gel precursor were formed at VFRRs of 10:1, 15:1, and 25:1. The total volumetric flow rate was held constant at 9.6 μL min^{-1} in all cases. Samples were collected at the device outlet for 55 min following 10 min of stabilization at each VFRR setting.

Off-Chip Formation of Hybrid Nanoparticles. Liposomes encapsulating the gel precursor were passed through a D-Salt polyacrylamide column (6 kDa cutoff), using PBS as the elution buffer, to remove the extravesicular gel precursor material from the sample. PDMS wells (0.625 in. diameter x 0.125 in. height) were stamped and cut from a cured PDMS sheet, and the wells were cleaned with ethanol followed by deionized water. They were dried with nitrogen before placing on a glass microscope slide. 0.5 mL aliquots of sample were added to each well and were irradiated with UV light at 365 nm from the Omnicure S2000 for 15 min.

Light Scattering and Asymmetric Flow Field-Flow Fractionation (AF4). An Eclipse Asymmetric Flow Field-Flow Fractionation (AF4) instrument integrated with a Dawn EOS multi-angle laser light scattering (MALLS) instrument was used for size fractionation and characterization of the liposomes and nanoparticles. The AF4 separation channel had a 190 μm spacer, and a regenerated cellulose membrane with a 10 kDa cutoff was used for the cross-flow partition. For the control liposomes, 10 mM PBS was used as the carrier solution. 10 μL of the liposome solution was loaded into the AF4 injection loop, and the fractionation was conducted with a 1 mLmin^{-1} channel flow and a 0.8 mL min^{-1} to 0.0 mL min^{-1} linearly decreasing crossflow gradient over 70 min. For the hybrid nanoparticles, a 5 mM PBS carrier solution, a 50 μL sample injection and a 0.6 mL min^{-1} to 0.0 mL min^{-1} linearly decreasing crossflow gradient over a 35 min elution period were used. MALLS data were collected simultaneously at 10 scattering angles on the eluting sample. A coated sphere model[83] was applied to the data using an estimated bilayer thickness of 5 nm to determine the geometric radii distributions of liposomes and hybrid nanoparticles.

Dynamic Light Scattering (DLS). A 90Plus/BI-MAS Particle Size Analyzer instrument was used for DLS measurements (Brookhaven Instruments). This instrument was equipped with a 15 mW solid state laser with a wavelength of 659 nm and measurements were made at 90° at a rate of one measurement per second. Prior to conducting measurements on a nanoparticle sample, it was centrifuged at 10,000 rpm for 4 min to remove any dust or aggregates. The supernatant was carefully

aspirated and diluted 1:10 in 0.02 μm filtered PBS, and the sample was added to a polymethylmethacrylate cuvette and placed in the measurement cell. Measurements were made over a series of temperatures.

Transmission Electron Microscopy (TEM). TEM of the hybrid nanoparticles was performed on a Philips EM 400T microscope operating at 120KV equipped with a Soft Imaging System CCD camera (Cantega 2K). TEM samples were prepared by dropping diluted solutions onto 400-mesh carbon-coated copper grids (from Ted Pella) and briefly air-drying the samples prior to measurements.

5.3. RESULTS AND DISCUSSION

5.3.1. Empty Liposomes in PBS

Empty liposomes, prepared in PBS without the hydrogel precursor, were synthesized in the microfluidic device as a calibration to determine the size ranges achieved at varying volumetric flow-rate ratios (VFRRs) with our device geometry and lipid formulation. At microfluidic length-scales, the mixing of miscible liquids is known to occur predominantly by molecular diffusion due to the laminar flow conditions. Therefore, in both the hydrodynamic focusing region and downstream in the diffusive mixing channel, IPA from the lipid stream will diffuse into the surrounding aqueous buffer stream and vice-versa. In turn, the concentration of lipid in the mixed liquid interface will exceed its critical aggregation concentration, causing the lipids to self-assemble into liposomes. In this process, the aqueous buffer and its contents will get encapsulated into the aqueous liposomal core.

The critical mixing time over which this self-assembly process occurs depends on the extent of focusing of the center stream. At lower focusing, or smaller VFRRs, the center lipid-IPA stream is relatively wide with a low surface-to-volume ratio between the lipid stream and sheath flows, requiring a longer diffusive mixing time to deplete the center stream. The prolonged lipid solubility results in the assembly of larger vesicles further downstream in the diffusive mixing channel while fewer vesicles form in the focusing region. At higher focusing, or larger VFRRs, the center stream is relatively narrow, which reduces the diffusion distance and enhances diffusive mixing in the hydrodynamic focusing region. Higher focusing also results

in a higher surface-to-volume ratio and a faster depletion of the center stream. This causes the self-assembly of smaller liposomes predominantly within the convective-diffusive focusing region as opposed to the downstream mixing channel. Control of these flow conditions enables predictable and repeatable production of liposomes with a given size distribution.

In our study, we formed liposomes at VFRRs of 10:1, 15:1, 20:1 and 25:1, and the collected samples were then characterized by AF4-MALLS. The size distribution of each VFRR sample is shown in Figure 5.3a. Here, for a given sample, each data point represents a MALLS measurement on a size-fractionated component; thereby, the overall size distribution is a more accurate characterization of the sample compared to that obtained from traditional static or dynamic light scattering[68]. The size distributions show the expected trend – i.e., an increase in VFRR results in a smaller average size of the liposomes[22]. For a simplified view of this trend, Figure 5.3b plots the average radius and polydispersity vs. VFRR. In calculating these averages, the sizes were weighted by the number density data from Figure 5.3a. The average radius and standard deviation of the distributions for the 10:1, 15:1, 20:1, and 25:1 samples were 65 ± 6 nm, 49 ± 7 nm, 44 ± 6 nm, and 41 ± 6 nm, respectively. These numbers indicate that each liposome population is narrowly dispersed, particularly when compared to other liposome preparation techniques[82]. At high VFRRs (> 20:1), the size varies only slightly, suggesting that we are approaching the lower limit of liposome size that can be produced for this formulation in our

microfluidic device. These results guided our selection of VFRR settings for the formation of the lipid-PNIPA hybrid nanoparticles.

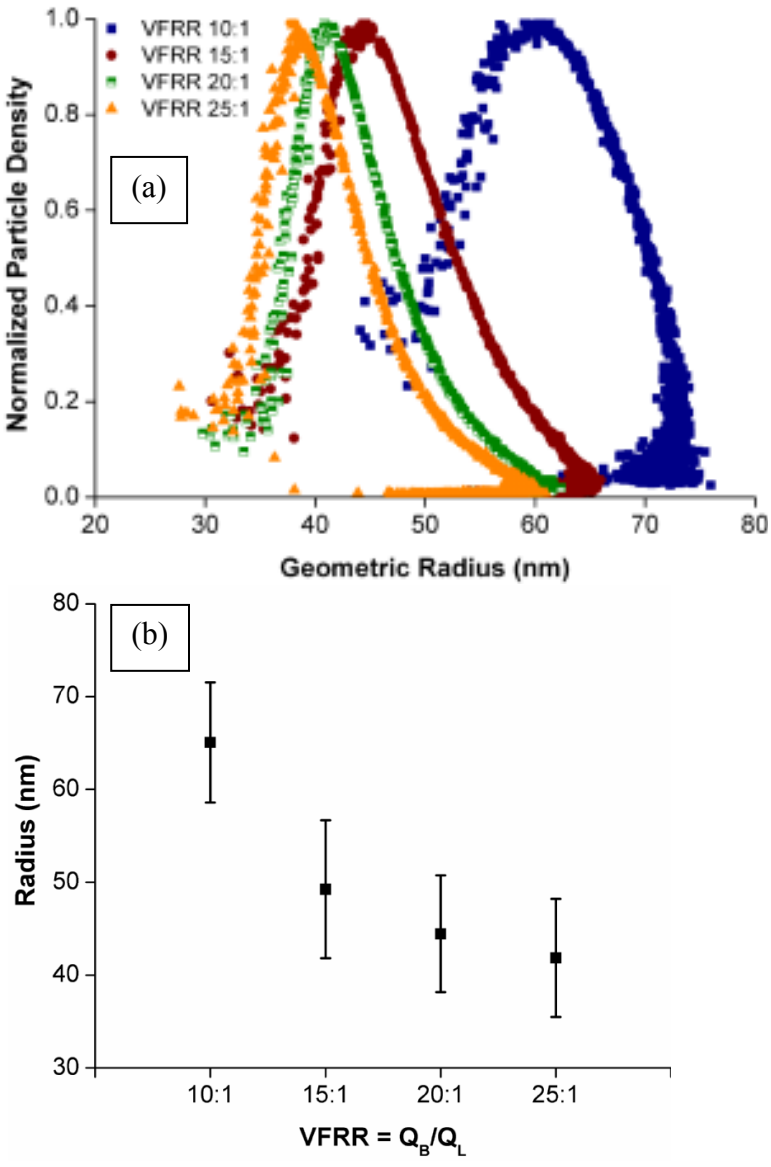

Figure 5.3. (a) Size distributions measured by AF4-MALLS of control liposome populations formed in PBS alone via hydrodynamic focusing at varying VFRRs. (b) The average outer vesicle radius and standard deviation of each population are shown. Q_B and Q_L denote the volumetric flow rates of the buffer and lipid/IPA, respectively.

5.3.2. Lipid-PNIPA Hybrid Nanoparticles

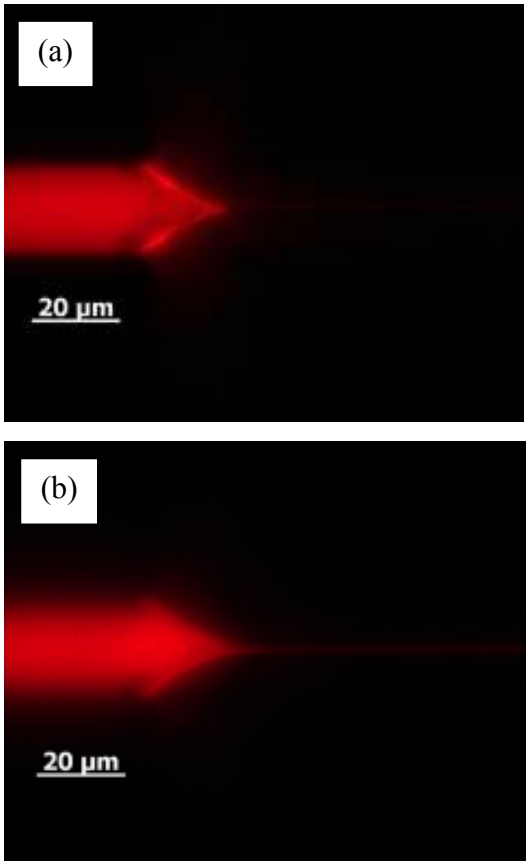

Figure 5.4. Interfacial buildup observed at the hydrodynamic focusing interface (a) the top of the channel, closer to the glass surface, and (b) in the middle of the channel.

Liposomes encapsulating the NIPA/MBA/DEAP hydrogel precursor solution were formed in continuous-flow runs at VFRRs of 10:1, 15:1, and 25:1. Compared to the liposomes in PBS alone, interfacial buildup (indicative of chemical incompatibility, such as phase separation) occurred more frequently at the hydrodynamic interface between the lipid and hydrogel precursor streams, especially closer to the borosilicate glass surface of the device (Figure 5.4). Such interfacial buildup was observed for all three VFRR settings but did not disrupt the directed assembly of precursor hybrid nanoparticles. However, this issue was more

problematic in trials with significantly higher hydrogel precursor concentrations (data not shown), which is one limitation of our technique.

The liposomes collected at the outlet of the microfluidic chip was purified by gel filtration and then UV polymerized to yield lipid-PNIPA hybrid nanoparticles (Figure 5.1). The size distributions of these nanoparticle samples were then measured by AF4-MALLS and are shown in Figure 5.5. The liposomes containing NIPA (before UV irradiation) were also characterized, and those results (Figure 5.5a) indicate structures with low polydispersities (comparable to empty liposomes). Polymerization does not alter the average size appreciably and the final lipid-PNIPA hybrid nanogels actually have more narrow size distributions (Figure 5.5b). This holds true at each of the applied VFRRs, spanning an overall size range of about 150 to 300 nm in diameter. The average radius and polydispersity for each VFRR is shown is Figure 5.6; these were (142±4) nm, (109±3) nm, and (92±5) nm for VFRRs of 10:1, 15:1, and 25:1, respectively.

An interesting point is that, at a given VFRR, liposomes containing NIPA were approximately twice the size of empty liposomes (compare Figures 5.3a and 5.5a). It is known from previous work that the liposome size obtained from microfluidics is sensitive to both the lipid composition as well as the presence of other solutes (such as dyes). Here, the presence of NIPA and other hydrogel precursors in the aqueous stream evidently dictates the change in size. The interfacial buildup in the presence of NIPA may also play a role in this context.

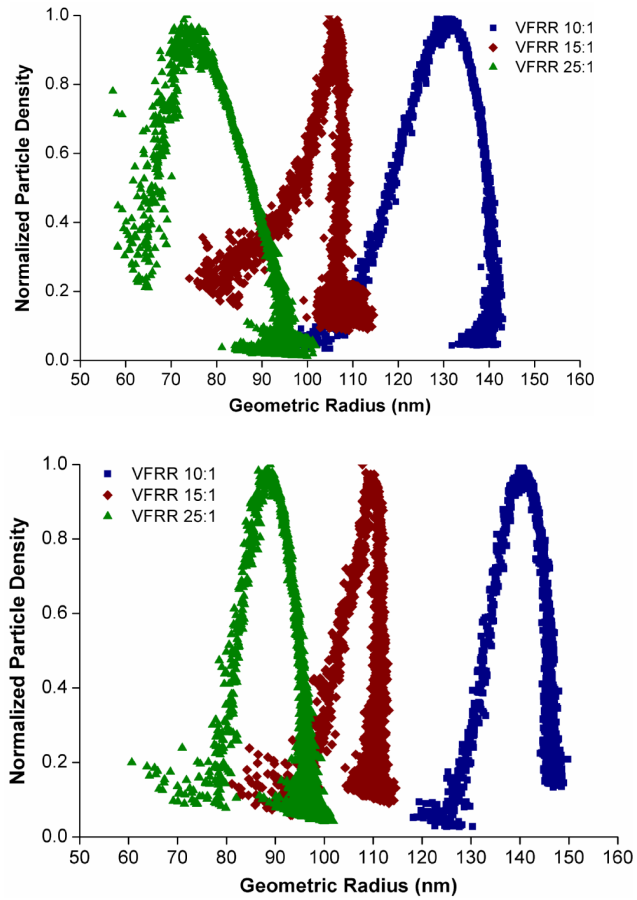

Figure 5.5. (a) Size distributions of lipid-NIPA liposomes; and (b) lipid-PNIPA hybrid nanoparticles formed by polymerizing the liposomes in (a).

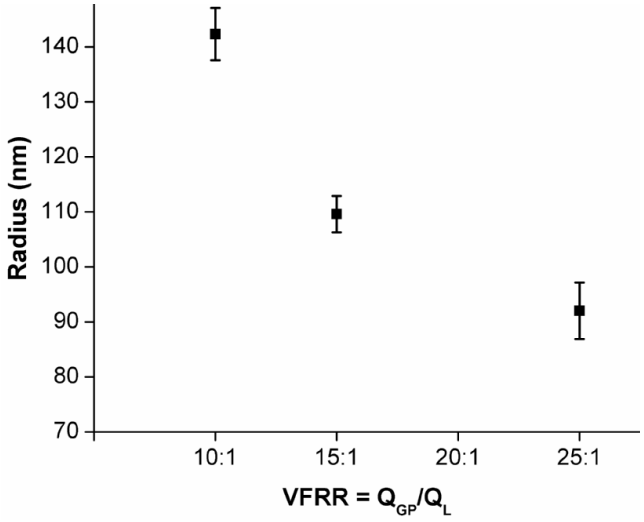

Figure 5.6. Average lipid-PNIPA hybrid nanoparticle size at varying VFRRs. Q_{GP} and Q_L denote the flow rates of the gel precursor and lipid solutions, respectively.

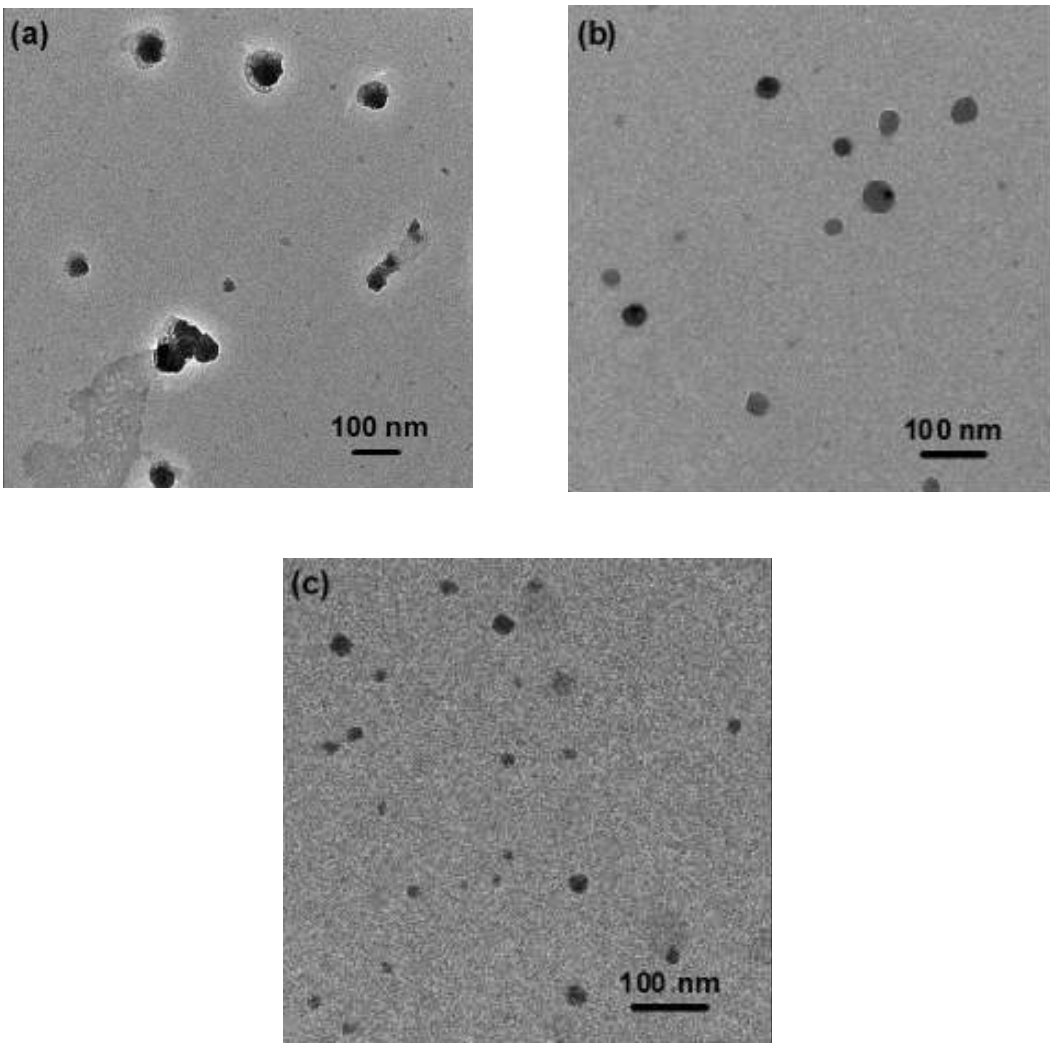

Figure 5.7. TEM micrographs of lipid-PNIPA hybrid nanoparticles formed at VFRRs of (a) 10:1, (b) 15:1, and (c) 25:1. The nanoparticles exhibit characteristics of solid spherical structures and show a trend of decreasing size with increasing VFRR.

The lipid-PNIPA hybrid nanoparticles formed by our approach showed a batch-to-batch reproducibility in size to within 5 % to 15 %., as measured by AF4-MALLS. The samples were also characterized by TEM (Figure 5.7). Each sample was air-dried on a TEM grid prior to imaging, and the micrographs therefore correspond to dehydrated nanoparticles. The hybrid nanoparticles were uniformly

solid and exhibited the round shape of the liposome envelope, which confirms the successful encapsulation and polymerization of the hydrogel precursor within the liposomal interior. The particle size exhibits a decrease with an increase in VFRR, as earlier demonstrated by AF4-MALLS. Note that the sizes are much smaller than those shown in Figure 4.6, and this is evidently because of the dehydration of the hydrogel nanoparticles.

5.3.3. Lipid-PNIPA Nanoparticle Temperature Sensitivity

To further validate our synthesis strategy, we probed the temperature-sensitivity of lipid-PNIPA hydrogel nanoparticles. These studies were done on particles synthesized at a VFRR of 10:1 using DLS. It is well-known that PNIPA exhibits a lower critical solution temperature (LCST) in water, and as a result, PNIPA hydrogels shrink when heated up to its LCST, which is ~ 32 °C. We therefore measured the size of lipid-PNIPA hydrogel nanoparticles over a range from 25 °C to 32 °C, and then at 37 °C (the latter being the physiological temperature at which these nanoparticles may potentially be applied). Prior to measurement at a given temperature, care was taken to ensure that the sample had reached thermal equilibrium. At each temperature, three measurement runs were performed and the average values of the hydrodynamic diameter D_h from DLS along with the standard deviations are plotted in Figure 5.8. D_h was 259.8±9.9 nm at 25 °C, 243.3±7.3 nm at 32 °C, and at 37 °C was 224±6.7 nm. The results show the characteristic temperature response of PNIPA, with the size decreasing past the LCST (32 °C). Similar results

have been reported by Levon et al. for lipid-PNIPA hybrid particles prepared by a bulk method.

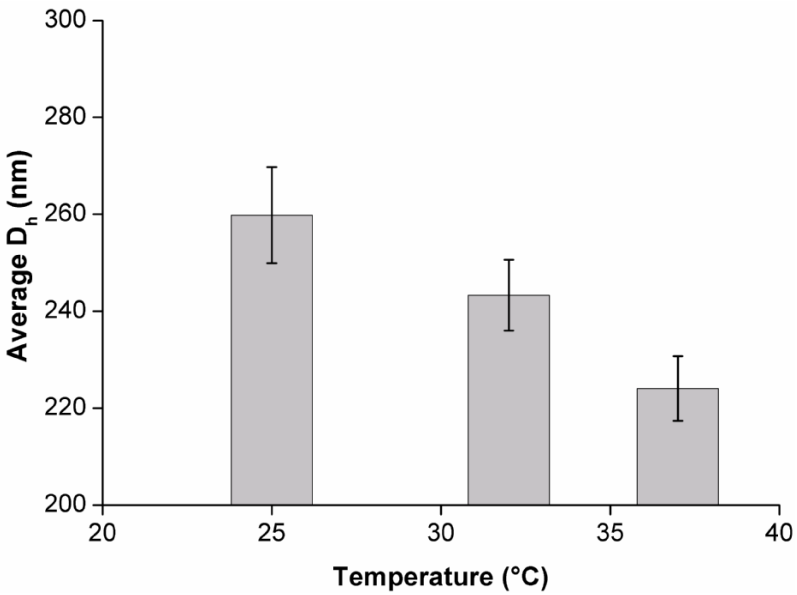

Figure 5.8. DLS data showing the effect of increasing temperature on the hydrodynamic diameter D_h of lipid-PNIPA hybrid nanoparticles prepared at a VFRR of 10:1.

A further interesting aspect is the effect of prolonged exposure at 37 °C on lipid-PNIPA hydrogel nanoparticles. Corresponding size data from DLS are shown in Figure 5.9. Each data point corresponds to the average D_h and standard variation from a 2.5 min measurement run. After 7.5 min exposure at 37 °C, the average D_h increased significantly, and this is indicative of nanoparticle aggregation. Similar behavior has also been previously reported by Levon et al.[72] for their bulk-prepared lipid-PNIPA particles. The increasing hydrophobicity of the PNIPA gel cores is believed to drive such aggregation.

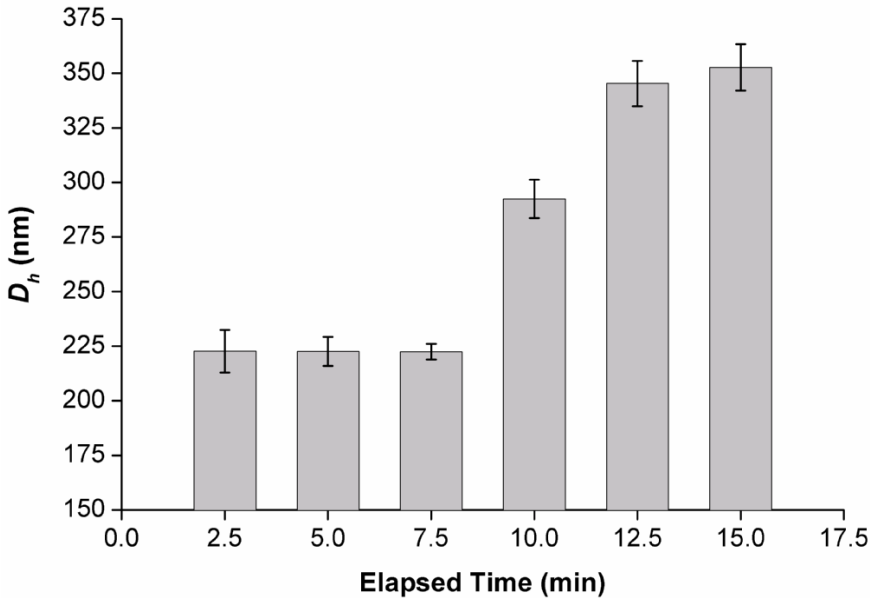

Figure 5.9. Time-lapse DLS data showing the effect of prolonged exposure to 37 °C on the hydrodynamic diameter D_h of lipid-PNIPA nanoparticles (VFRR of 10:1).

5.3.4. Lipid-PNIPA Nanoparticle Stability

Liposome-PNIPA nanoparticles were monitored for stability after formation. Fluorescence micrographs of particles two weeks after formation (Figure 5.10a) confirm that the particles are discrete and unaggregated. TEM measurements in Figure 5.10b show hybrid nanoparticles made at a VFRR 15:1 after two months. The nanoparticles generally show the same solid, spherical structure as the initially polymerized sample shown in Figure 5.7b, further confirming their stability and robustness. DLS measurements made on samples after 4 months also verified that the sizes remained consistent, which is likely due to the lipid bilayer coating preventing aggregation of the PNIPA nanogel cores. It should be noted that the DCP component of the lipid formulation has a negative charge, which confers electrostatic stability to the resulting liposomes as well as to the lipid-PNIPA nanoparticles.

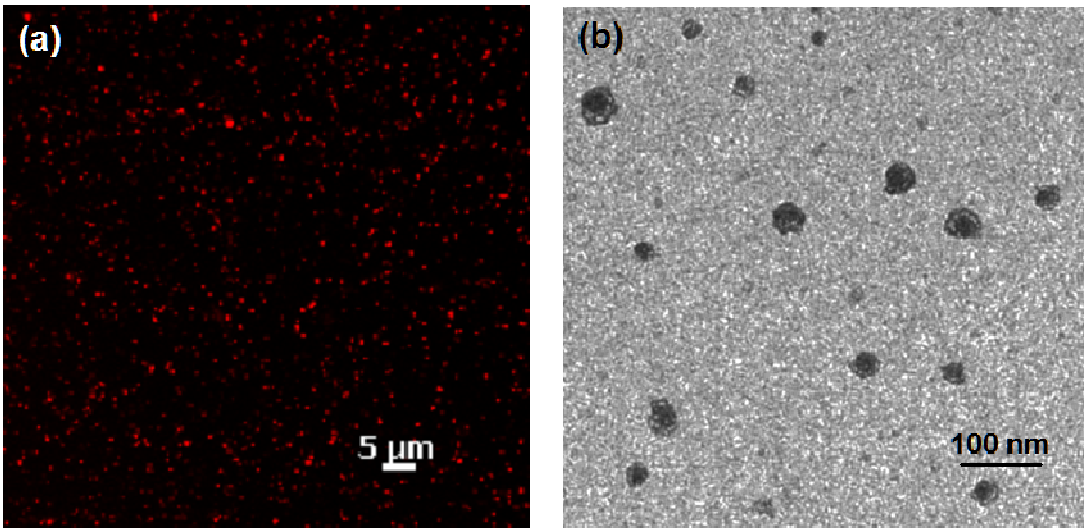

Figure 5.10. Stability of the lipid-PNIPA hybrid nanoparticles: (a) Epifluorescence micrograph taken two weeks after sample formation shows that the nanoparticles remain unaggregated. (b) TEM of the VFRR 15:1 sample two months after formation shows that the particles still retain similar structure and size, comparable to the original sample in Figure 5.7b.

Bulk preparations of lipid-hydrogel nanoparticles typically involve the use of a single formulation of lipid and hydrogel precursor to produce a single vesicle population with a particular size distribution determined by the application of several size-altering post-processing steps, which can decrease yield, increase cost and introduce biological compatibility issues. Using our microfluidic method, we synthesized relatively monodisperse populations of lipid-PNIPA hybrid nanoparticles from a single formulation without size-altering post-processing. Through precise variation of microfluidic mixing conditions, our method should be able to produce nanoparticle populations with any intended size within a finite range from an initial formulation, limited primarily by the chemical compatibility of the precursor solutions at the fluidic interface. Our approach could be useful in therapeutic agent delivery and cellular uptake applications, which often require different carrier

materials and sizes to target different types of cells. With the myriad of polymers and lipids commercially available and the interest in tailoring different types of nanoparticles for various applications[101], the development of a more standardized and controlled formation method such as the presented model system would be advantageous. We expect that this system could be adapted and optimized for the microfluidic-directed synthesis of hybrid nanoparticles derived from other soft matter precursors of present interest.

5.4. CONCLUSIONS

We have presented a microfluidic focusing method to direct the assembly of lipid-PNIPA hybrid nanoparticles. By varying the microfluidic mixing conditions, we were able to control the size of the liposome molds that encapsulated the gel precursor, which thereby determined the sizes of the resultant hybrid nanoparticles. Using light scattering and TEM, we verified that our method produced narrowly-dispersed populations of lipid-hydrogel hybrid nanoparticles over a size range pertinent to targeted delivery and controlled release applications. Our method can be further improved through on-chip integration of the off-chip formation steps; however the main objective of our work is to demonstrate the utility of a microfluidic-directed approach towards hybrid nanoparticles. We believe that this microfluidic approach may be customized for the synthesis of a wide variety of soft nanoparticles that are currently prepared via bulk methods.

6. CONCLUSIONS AND RECOMMENDATIONS

6.1. CONCLUSIONS

We have presented three studies that focus on the development of methods for the self-assembly of multiple material soft matter nanoparticles, highlighting the use of nanoscale phospholipid vesicles as reaction vessels for supramolecular assembly of nanoscale hydrogel structures. While liposomes were previously applied in this capacity for the self-assembly of larger microparticle structures, few had investigated the use of liposomes for the synthesis of nanoparticles. Soft matter nanoparticles are recognized for possessing many unique and potentially useful properties owing to their small size, especially in the areas of controlled release and therapeutics.

We first used liposomes to template the supramolecular assembly of calcium alginate gel nanoparticles using a gentle bulk synthesis procedure compared with the commonly applied synthesis techniques. Liposomes were self-assembled in a sodium alginate precursor solution by bulk solvent-injection, and after purification the lipid bilayer membrane was permeabilized at its transition temperature to facilitate the diffusion of calcium ions from the surrounding buffer into the liposome core to ionically crosslink the encapsulated sodium alginate into a calcium alginate gel. Upon lipid removal, the resultant nanogels were verified to be similar in size and shape to the original liposomes. We further demonstrated that the size of the resultant gels could be tailored by modifying the initial lipid formulation, which by extension altered the self-assembled liposome template size. Depending on the desired

application, the bare calcium-alginate nanogels or the hybrid lipid-alginate nanoparticles could be produced.

The potential improvement over size control and yield of the bulk liposome-templated alginate nanogel preparation was investigated by adapting a microfluidic directed self-assembly method that was previously shown to improve the control over the self-assembly of nanoscale liposomes. Modifications to the lipid and sodium alginate formulations were made to enable continuous formation of liposomes with encapsulated alginate with microfluidic hydrodynamic focusing. By adjusting the microfluidic mixing conditions of the lipid and alginate precursor solutions, we produced three relatively monodisperse populations of liposomes with discrete size distributions, however the encapsulation efficiency of sodium alginate was very low. These findings suggested that this microfluidic self-assembly method would be better suited for hydrogel materials based on smaller oligomer or monomer precursor materials.

Finally we used the microfluidic directed self-assembly method to produce lipid-hydrogel hybrid nanoparticles with a commonly used photopolymerizable hydrogel monomer-based, PNIPA. From a single lipid and PNIPA precursor formulation, we produced three highly monodisperse and discrete populations of nanoscale liposomes encapsulating the hydrogel monomer precursor. The liposome cores were UV polymerized and the resultant lipid-PNIPA hybrid nanoparticles were verified to be of the same size and shape as the liposomes as well as retaining the

temperature-sensitive properties known of the PNIPA polymer. We foresee the extension of this continuous microfluidic approach to the directed self-assembly of other lipid-polymer hybrid nanoparticle systems that have been limited to bulk synthesis methods.

6.2. Recommendations for Future Work

6.2.1. Microfluidic Device Optimization

The chemical incompatibilities we encountered at the focusing interface of the microfluidic channel occurred mainly at the glass surface of the device. The channel depths in our device were approximately 39 μm deep, thus the effect of the several microns of transient buildup close to the glass surface accounted for approximately 10% of the mixing region. Recently we learned that with respect to microfluidic mixing, fabrication of microchannels with a small width-to-depth aspect ratio can significantly increase the uniformity of the hydrodynamic focusing interface[54]. A deeper microchannel would reduce the fraction of sample that may be affected by the chemical incompatibilities, with the added advantage of increased sample output with little sample dilution[82]. Alternatively, increasing the channel width would also lead to a higher sample throughput, but with a lower resultant nanoparticle concentration due to the higher VFRRs required to achieve the same focusing conditions as a device with a smaller channel width. We believe that these device modifications would greatly improve device robustness and reusability, while also improving ease of sample production and the reproducibility of samples produced from run to run.

6.2.2. Formulation Optimization for Microfluidic Directed Synthesis

We studied several formulations for the self-assembly of lipid-PNIPA nanoparticles, however a more systematic investigation into the effect of initial lipid and hydrogel precursor formulations on the resultant hybrid nanoparticle population size and composition would be useful. The duration of UV polymerization required for gelation of the encapsulated hydrogel precursor should also be optimized to the shortest time required for free radical polymerization. These studies would improve the efficiency and applicability of our method.

The polymerization of PNIPA can be initiated with several different photoinitiators as well as chemical initiators. Chemical initiators, such as the strong oxidizer ammonium persulfate, have been used for polymerization of PNIPA but they tend to be highly toxic and therefore an unfavorable choice for our intended applications. In Chapter 5 we used a small quantity of DEAP, a significantly less toxic hydrophobic photoinitiator, which was sufficient in initiating polymerization but had limited solubility in the hydrogel precursor solution that was composed of hydrophilic monomers. The next formulation improvement might be to use a hydrophilic photoinitiator such as riboflavin, a photosensitive vitamin that has been used in the polymerization of acrylamide[102].

An alternative photoinitiator to try would be 2-hydroxy-1-[4-[2-hydroxyethoxy)phenyl]-2-methyl-1-propanone (Irgacure 2959), which is most commonly used for photopolymerization of hydrogels that are used for *in situ* cellular

or tissue engineering research[103], which has been found to be the least harmful to a broad range of mammalian cell types compared to others[104-107]. Irgacure 2959 can also be used in a lower concentration than the DEAP, potentially improving the solubility in the hydrogel precursor mixture. With a more soluble photoinitiator we may be able to optimize the concentration used to reduce the polymerization time required for the formation of PNIPA.

6.2.3. Integration of Off-Chip Processing Steps

Our work has focused on the initial microfluidic mixing self-assembly step, which is perhaps the most critical in determining the size and composition of the resultant nanoparticles. However the ultimate goal is to completely automate this method, which would require the integration of the sample purification and free radical polymerization steps on-chip. One possible method for sample purification would involve adding several rinsing steps to the device to dilute the vesicles downstream after self-assembly and encapsulation. The unencapsulated hydrogel precursor molecules would diffuse outward into the fresh buffer while the larger liposomes would remain focused in center of the mixing channel due to their smaller diffusion coefficients. Following the purification step, UV irradiation of the sample would be integrated downstream.

6.2.4. Encapsulation of Model Drug

We have demonstrated a method that produces highly monodisperse hybrid nanoparticles, and the next step is to study the encapsulation of a model drug such as

a fluorescent dye or a protein such as bovine serum albumin. We believe our particle synthesis method is relatively gentle, however the hydrogel precursor solution is known to be toxic, and therefore the effect on encapsulated biomolecules must be investigated. An alternative, less toxic method of encapsulation may be to template the hydrogel nanoparticles first, incubate them with the encapsulant of interest, and then re-attach a lipid shell around the nanogel. This would promote uniform encapsulation and structure of the particles, which is critical for precise controlled release.

6.2.5. Cellular Nanotoxicity

PNIPA has been studied extensively for its unique thermosensitive material properties that are considered to be potentially useful for the triggered release of drugs near physiological temperatures[104,108]. To this end, it is important to understand the interactions these liposome-PNIPA nanoparticles have with cells and the potential limitations associated with their application. It is well-known that size is a critical parameter in determining the fate of nanoparticles when using them for targeted delivery or controlled release. The microfluidic approach we have demonstrated would enable us to systematically study the effects that varying nanoparticle size, composition, and concentration may have on cellular uptake, metabolic processes, and cell viability. This type of toxicity data is badly needed before the practical application of these and many other types of nanoparticles can be realized[5].

6.2.6. Additional Soft Hybrid Systems

One main goal in developing this microfluidic system is to have an adaptable method for the formation of other hybrid nanoparticle systems. Within our current lipid-PNIPA system, the overall attainable size range of the nanoparticles could be adjusted by changing the initial lipid formulation, which would translate into a different liposome template size due to the fundamentally altered self-assembly conditions.

Given the results of the microfluidic directed synthesis of lipid-alginate hybrid nanoparticles, our method may be limited to hydrogel materials based on small monomer gel precursors or oligomers of known molecular weight that can be crosslinked into a supramolecular assembly. Within this subclass of materials, there are still large number relevant to the synthesis of particles for pharmaceutical applications that we could investigate[45], including photopolymerizable materials.

One particular material of interest is poly(ethylene glycol) diacrylate (PEG-DA), which can be obtained at relatively small known molecular weights and has been used to synthesize lipid-PEG hybrid nanoparticles[93]. PEG-DA, a derivative of PEG, is a familiar nontoxic polymer currently used in a number of drug delivery and cell-based studies. PEG-DA can also be functionalized with a variety of molecules such as peptides, which offers another degree of versatility when considering the design of a nanoparticle delivery system.

REFERENCES

[1] "http://www.cybercolloids.net/library/alginate/structure.php, http://blog.khymos.org/wp-content/2006/09/calcium-alginate.jpg.".

[2] Lehn, J. "Supramolecular chemistry - scope and perspectives molecules, supermolecules, and molecular devices." *Angewandte Chemie* **1988**, *27*, 89-112.

[3] Xia, Y. N.; Whitesides, G. M. "Soft lithography." *Angewandte Chemie-International Edition* **1998**, *37*, 551-575.

[4] Whitesides, G. M.; Mathias, J. P.; Seto, C. T. "Molecular Self-Assembly and Nanochemistry - a Chemical Strategy for the Synthesis of Nanostructures." *SCIENCE Nagatsuta, Yokohama, Kanagawa 2268503, Japan Tokyo Inst Technol, Chem Resources Lab, Midori Ku, Yokohama, Kanagawa 2268503, Japan* **1991**, *254*, 1312-1319.

[5] Sanvicens, N.; Marco, M. P. "Multifunctional nanoparticles - properties and prospects for their use in human medicine." *Trends in Biotechnology* **2008**, *26*, 425-433.

[6] Kohane, D. S. "Microparticles and nanoparticles for drug delivery." *Biotechnology and Bioengineering* **2007**, *96*, 203-209.

[7] Naha, P. C.; Casey, A.; Tenuta, T.; Lynch, I.; Dawson, K. A.; Byrne, H. J.; Davoren, M. "Preparation, characterization of NIPAM and NIPAM/BAM copolymer nanoparticles and their acute toxicity testing using an aquatic test battery." *Aquatic Toxicology* **2009**, *92*, 146-154.

[8] Jin, T.; Pennefather, P.; Lee, P. I. "Lipobeads: A hydrogel anchored lipid vesicle system." *Febs Letters* **1996**, *397*, 70-74.

[9] Zhang, L. F.; Chan, J. M.; Gu, F. X.; Rhee, J. W.; Wang, A. Z.; Radovic-Moreno, A. F.; Alexis, F.; Langer, R.; Farokhzad, O. C. "Self-assembled lipid-polymer hybrid nanoparticles: A robust drug delivery platform." *ACS Nano* **2008**, *2*, 1696-1702.

[10] Buck, S.; Pennefather, P. S.; Xue, H. Y.; Grant, J.; Cheng, Y. L.; Allen, C. J. "Engineering lipobeads: Properties of the hydrogel core and the lipid bilayer shell." *Biomacromolecules* **2004**, *5*, 2230-2237.

[11] Thevenot, J.; Troutier, A. L.; David, L.; Delair, T.; Ladaviere, C. "Steric stabilization of lipid/polymer particle assemblies by poly(ethylene glycol)-lipids." *Biomacromolecules* **2007**, *8*, 3651-3660.

[12] Wong, H. L.; Rauth, A. M.; Bendayan, R.; Manias, J. L.; Ramaswamy, M.; Liu, Z. S.; Erhan, S. Z.; Wu, X. Y. "A new polymer-lipid hybrid nanoparticle system increases cytotoxicity of doxorubicin against multidrug-resistant human breast cancer cells." *Pharmaceutical Research* **2006**, *23*, 1574-1585.

[13] Kazakov, S.; Kaholek, M.; Teraoka, I.; Levon, K. "UV-induced gelation on nanometer scale using liposome reactor." *MACROMOLECULES* **2002**, *35*, 1911-1920.

[14] Patton, J. N.; Palmer, A. F. "Photopolymerization of bovine hemoglobin entrapped nanoscale hydrogel particles within liposomal reactors for use as an artificial blood substitute." *Biomacromolecules* **2005**, *6*, 414-424.

[15] Schillemans, J. P.; Flesch, F. M.; Hennink, W. E.; van Nostrum, C. F. "Synthesis of bilayer-coated nanogels by selective cross-linking of monomers inside liposomes." *MACROMOLECULES* **2006**, *39*, 5885-5890.

[16] Van Thienen, T. G.; Lucas, B.; Flesch, F. M.; van Nostrum, C. F.; Demeester, J.; De Smedt, S. C. "On the synthesis and characterization of biodegradable dextran nanogels with tunable degradation properties." *MACROMOLECULES* **2005**, *38*, 8503-8511.

[17] Jahn, A.; Reiner, J. E.; Vreeland, W. N.; DeVoe, D. L.; Locascio, L. E.; Gaitan, M. "Preparation of nanoparticles by continuous-flow microfluidics." *Journal of Nanoparticle Research* **2008**, *10*, 925-934.

[18] Rondeau, E.; Cooper-White, J. J. "Biopolymer microparticle and nanoparticle formation within a microfluidic device." *Langmuir* **2008**, *24*, 6937-6945.

[19] Karnik, R.; Gu, F.; Basto, P.; Cannizzaro, C.; Dean, L.; Kyei-Manu, W.; Langer, R.; Farokhzad, O. C. "Microfluidic platform for controlled synthesis of polymeric nanoparticles." *Nano Letters* **2008**, *8*, 2906-2912.

[20] Farokhzad, O. C.; Langer, R. "Impact of Nanotechnology on Drug Delivery." *ACS Nano* **2009**, *3*, 16-20.

[21] Raemdonck, K.; Demeester, J.; De Smedt, S. "Advanced nanogel engineering for drug delivery." *Soft Matter* **2009**, *5*, 707-715.

[22] Jahn, A.; Vreeland, W. N.; DeVoe, D. L.; Locascio, L. E.; Gaitan, M. "Microfluidic directed formation of liposomes of controlled size." *Langmuir* **2007**, *23*, 6289-6293.

[23] Kohn, R. “Ion Binding on Polyuronates - Alginate and Pectin.” *Pure and Applied Chemistry* **1975**, *42*, 371-397.

[24] Gombotz, W. R.; Wee, S. F. “Protein release from alginate matrices.” *Advanced Drug Delivery Reviews* **1998**, *31*, 267-285.

[25] Augst, A. D.; Kong, H. J.; Mooney, D. J. “Alginate hydrogels as biomaterials.” *Macromolecular Bioscience* **2006**, *6*, 623-633.

[26] Fundueanu, G.; Nastruzzi, C.; Carpov, A.; Desbrieres, J.; Rinaudo, M. “Physico-chemical characterization of Ca-alginate microparticles produced with different methods.” *Biomaterials* **1999**, *20*, 1427-1435.

[27] Darrabie, M. D.; Kendall, W. F.; Opara, E. C. “Effect of alginate composition and gelling cation on micro-bead swelling.” *Journal of Microencapsulation* **2006**, *23*, 29-37.

[28] Tonnesen, H. H.; Karlsen, J. “Alginate in drug delivery systems.” *Drug Development and Industrial Pharmacy* **2002**, *28*, 621-630.

[29] Polk, A.; Amsden, B.; Deyao, K.; Peng, T.; Goosen, M. F. A. “Controlled-Release of Albumin from Chitosan-Alginate Microcapsules.” *Journal of Pharmaceutical Sciences* **1994**, *83*, 178-185.

[30] Ennett, A. B.; Kaigler, D.; Mooney, D. J. “Temporally regulated delivery of VEGF in vitro and in vivo.” *Journal of Biomedical Materials Research Part* **2006**, *79A*, 176-184.

[31] Fragonas, E.; Valente, M.; Pozzi-Mucelli, M.; Toffanin, R.; Rizzo, R.; Silvestri, F.; Vittur, F. “Articular cartilage repair in rabbits by using suspensions of allogenic chondrocytes in alginate.” *Biomaterials* **2000**, *21*, 795-801.

[32] Hauselmann, H. J.; Fernandes, R. J.; Mok, S. S.; Schmid, T. M.; Block, J. A.; Aydelotte, M. B.; Kuettner, K. E.; Thonar, E. “Phenotypic Stability of Bovine Articular Chondrocytes after Long-Term Culture in Alginate Beads.” *Journal of Cell Science* **1994**, *107*, 17-27.

[33] Rowley, J. A.; Madlambayan, G.; Mooney, D. J. “Alginate hydrogels as synthetic extracellular matrix materials.” *Biomaterials* **1999**, *20*, 45-53.

[34] Kushner, D. J. “Self-Assembly of Biological Structures.” *Bacteriol. Rev.* **1969**, *33*, 302-&.

[35] Misteli, T. “The concept of self-organization in cellular architecture.” *Journal of Cell Biology* **2001**, *155*, 181-185.

[36] Andresen, T. L.; Jensen, S. S.; Jorgensen, K. “Advanced strategies in liposomal cancer therapy: Problems and prospects of active and tumor specific drug release.” *Progress in Lipid Research* **2005**, *44*, 68-97.

[37] Lian, T.; Ho, R. J. Y. “Trends and developments in liposome drug delivery systems.” *Journal of Pharmaceutical Sciences* **2001**, *90*, 667-680.

[38] Pinto-Alphandary, H.; Andremont, A.; Couvreur, P. “Targeted delivery of antibiotics using liposomes and nanoparticles: research and applications.” *International Journal of Antimicrobial Agents* **2000**, *13*, 155-168.

[39] Vreeland, W. N.; Locascio, L. E. “Using bioinspired thermally triggered liposomes for high-efficiency mixing and reagent delivery in microfluidic devices.” *Analytical Chemistry* **2003**, *75*, 6906-6911.

[40] Kraske, W. V.; Mountcastle, D. B. “Effects of cholesterol and temperature on the permeability of dimyristoylphosphatidylcholine bilayers near the chain melting phase transition.” *Biochimica Et Biophysica Acta-Biomembranes* **2001**, *1514*, 159-164.

[41] Bagatolli, L. A.; Gratton, E. “Two photon fluorescence microscopy of coexisting lipid domains in giant unilamellar vesicles of binary phospholipid mixtures.” *Biophysical Journal* **2000**, *78*, 290-305.

[42] Xiang, T. X.; Anderson, B. D. “Phase structures of binary lipid bilayers as revealed by permeability of small molecules.” *Biochimica Et Biophysica Acta-Biomembranes* **1998**, *1370*, 64-76.

[43] Westhaus, E.; Messersmith, P. B. “Triggered release of calcium from lipid vesicles: a bioinspired strategy for rapid gelation of polysaccharide and protein hydrogels.” *Biomaterials* **2001**, *22*, 453-462.

[44] Vihola, H.; Laukkanen, A.; Valtola, L.; Tenhu, H.; Hirvonen, J. “Cytotoxicity of thermosensitive polymers poly(N-isopropylacrylamide), poly(N-vinylcaprolactam) and amphiphilically modified poly(N-vinylcaprolactam).” *Biomaterials* **2005**, *26*, 3055-3064.

[45] Hamidi, M.; Azadi, A.; Rafiei, P. “Hydrogel nanoparticles in drug delivery.” *Advanced Drug Delivery Reviews* **2008**, *60*, 1638-1649.

[46] Liu, Q. F.; Zhang, P.; Qing, A. X.; Lan, Y. X.; Lu, M. G. “Poly(N-isopropylacrylamide) hydrogels with improved shrinking kinetics by RAFT polymerization.” *POLYMER* **2006**, *47*, 2330-2336.

[47] Kratz, K.; Hellweg, T.; Eimer, W. “Structural changes in PNIPAM microgel particles as seen by SANS, DLS, and EM techniques.” *POLYMER* **2001**, *42*, 6631-6639.

[48] Karg, M.; Hellweg, T. “New "smart" poly(NIPAM) microgels and nanoparticle microgel hybrids: Properties and advances in characterisation.” *CURRENT OPINION IN COLLOID & INTERFACE SCIENCE USA Univ Wisconsin, Dept Chem Engn, Madison, WI 53706 USA Univ Wisconsin, Rheol Res Ctr, Madison, WI 53706 USA* **2009**, *14*, 438-450.

[49] Debord, J. D.; Lyon, L. A. “Synthesis and characterization of pH-responsive copolymer microgels with tunable volume phase transition temperatures.” *Langmuir* **2003**, *19*, 7662-7664.

[50] Weigl, B. H.; Yager, P. “Microfluidics - Microfluidic diffusion-based separation and detection.” *SCIENCE Nagatsuta, Yokohama, Kanagawa 2268503, Japan Tokyo Inst Technol, Chem Resources Lab, Midori Ku, Yokohama, Kanagawa 2268503, Japan* **1999**, *283*, 346-347.

[51] Atencia, J.; Beebe, D. J. “Controlled microfluidic interfaces.” *Nature* **2005**, *437*, 648-655.

[52] Knight, J. B.; Vishwanath, A.; Brody, J. P.; Austin, R. H. “Hydrodynamic focusing on a silicon chip: Mixing nanoliters in microseconds.” *Physical Review Letters* **1998**, *80*, 3863-3866.

[53] Brody, J. P.; Yager, P.; Goldstein, R. E.; Austin, R. H. “Biotechnology at low Reynolds numbers.” *Biophysical Journal* **1996**, *71*, 3430-3441.

[54] Park, H. Y.; Qiu, X. Y.; Rhoades, E.; Korlach, J.; Kwok, L. W.; Zipfel, W. R.; Webb, W. W.; Pollack, L. “Achieving uniform mixing in a microfluidic device: Hydrodynamic focusing prior to mixing.” *Analytical Chemistry* **2006**, *78*, 4465-4473.

[55] Jahn, A.; Vreeland, W. N.; Gaitan, M.; Locascio, L. E. “Controlled vesicle self-assembly in microfluidic channels with hydrodynamic focusing.” *Journal of the American Chemical Society* **2004**, *126*, 2674-2675.

[56] Fraunhofer, W.; Winter, G.; Coester, C. “Asymmetrical flow field-flow fractionation and multiangle light scattering for analysis of gelatin nanoparticle drug carrier systems.” *Analytical Chemistry* **2004**, *76*, 1909-1920.

[57] Ge, L. Q.; Mohwald, H.; Li, J. B. "Phospholipid liposomes stabilized by the coverage of polyelectrolyte." *Colloids and Surfaces a-Physicochemical and Engineering Aspects* **2003**, *221*, 49-53.

[58] Langer, R. "New Methods of Drug Delivery." *SCIENCE Nagatsuta, Yokohama, Kanagawa 2268503, Japan Tokyo Inst Technol, Chem Resources Lab, Midori Ku, Yokohama, Kanagawa 2268503, Japan* **1990**, *249*, 1527-1533.

[59] Qiu, Y.; Park, K. "Environment-sensitive hydrogels for drug delivery." *Advanced Drug Delivery Reviews* **2001**, *53*, 321-339.

[60] Calvo, P.; VilaJato, J. L.; Alonso, M. J. "Evaluation of cationic polymer-coated nanocapsules as ocular drug carriers." *International Journal of Pharmaceutics* **1997**, *153*, 41-50.

[61] Saltzman, W. M.; Olbricht, W. L. "Building drug delivery into tissue engineering." *Nature Reviews Drug Discovery* **2002**, *1*, 177-186.

[62] Mainardes, R. M.; Silva, L. P. "Drug delivery systems: Past, present, and future." *Current Drug Targets* **2004**, *5*, 449-455.

[63] Sershen, S.; West, J. "Implantable, polymeric systems for modulated drug delivery." *Advanced Drug Delivery Reviews* **2002**, *54*, 1225-1235.

[64] Allen, T. M.; Cullis, P. R. "Drug delivery systems: Entering the mainstream." *SCIENCE Nagatsuta, Yokohama, Kanagawa 2268503, Japan Tokyo Inst Technol, Chem Resources Lab, Midori Ku, Yokohama, Kanagawa 2268503, Japan* **2004**, *303*, 1818-1822.

[65] Drummond, D. C.; Meyer, O.; Hong, K. L.; Kirpotin, D. B.; Papahadjopoulos, D. "Optimizing liposomes for delivery of chemotherapeutic agents to solid tumors." *Pharmacological Reviews* **1999**, *51*, 691-743.

[66] Kong, G.; Braun, R. D.; Dewhirst, M. W. "Hyperthermia enables tumor-specific nanoparticle delivery: Effect of particle size." *Cancer Research* **2000**, *60*, 4440-4445.

[67] Prabha, S.; Zhou, W. Z.; Panyam, J.; Labhasetwar, V. "Size-dependency of nanoparticle-mediated gene transfection: studies with fractionated nanoparticles." *International Journal of Pharmaceutics* **2002**, *244*, 105-115.

[68] Wyatt, P. J. "Submicrometer particle sizing by multiangle light scattering following fractionation." *Journal of Colloid and Interface Science* **1998**, *197*, 9-20.

[69] Wyatt, P. J.; Villapando, D. N. "High-precision measurement of submicrometer particle size distributions." *Langmuir* **1997**, *13*, 3913-3914.

[70] Monshipouri, M.; Rudolph, A. S. "Liposome-Encapsulated Alginate - Controlled Hydrogel Particle Formation and Release." *Journal of Microencapsulation* **1995**, *12*, 117-127.

[71] Jesorka, A.; Markstrom, M.; Orwar, O. "Controlling the internal structure of giant unilamellar vesicles by means of reversible temperature dependent sol-gel transition of internalized poly (N-isopropyl acrylamide)." *Langmuir* **2005**, *21*, 1230-1237.

[72] Kazakov, S.; Levon, K. "Liposome-nanogel structures for future pharmaceutical applications." *Current Pharmaceutical Design* **2006**, *12*, 4713-4728.

[73] Kazakov, S.; Kaholek, M.; Kudasheva, D.; Teraoka, I.; Cowman, M. K.; Levon, K. "Poly(N-isopropylacrylamide-co-1-vinylimidazole) hydrogel nanoparticles prepared and hydrophobically modified in liposome reactors: Atomic force microscopy and dynamic light scattering study." *Langmuir* **2003**, *19*, 8086-8093.

[74] Bagatolli, L. A.; Gratton, E. "A correlation between lipid domain shape and binary phospholipid mixture composition in free standing bilayers: A two-photon fluorescence microscopy study." *Biophysical Journal* **2000**, *79*, 434-447.

[75] Viallat, A.; Dalous, J.; Abkarian, M. "Giant lipid vesicles filled with a gel: Shape instability induced by osmotic shrinkage." *Biophysical Journal* **2004**, *86*, 2179-2187.

[76] Plant, A. L.; Locasciobrown, L.; Haller, W.; Durst, R. A. "Immobilization of Binding-Proteins on Nonporous Supports - Comparison of Protein Loading, Activity, and Stability." *Applied Biochemistry and Biotechnology* **1991**, *30*, 83-98.

[77] Batzri, S.; Korn, E. D. "Single Bilayer Liposomes Prepared without Sonication." *Biochim. Biophys. Acta* **1973**, *298*, 1015-1019.

[78] Yu, Y. L.; DesLauriers, P. J.; Rohlfing, D. C. "SEC-MALS method for the determination of long-chain branching and long-chain branching distribution in polyethylene." *POLYMER* **2005**, *46*, 5165-5182.

[79] Kaasgaard, T.; Mouritsen, O. G.; Jorgensen, K. "Freeze/thaw effects on lipid-bilayer vesicles investigated by differential scanning calorimetry." *Biochimica Et Biophysica Acta-Biomembranes* **2003**, *1615*, 77-83.

[80] Lasic, D. D. *Liposomes: From Physics to Applications*; Elsevier: Amsterdam, 1993.

[81] Bajpai, S. K.; Sharma, S. "Investigation of swelling/degradation behaviour of alginate beads crosslinked with Ca2+ and Ba2+ ions." *Reactive & Functional Polymers* **2004**, *59*, 129-140.

[82] Jahn, A.; Stavis, S. M.; Hong, J. S.; Vreeland, W. N.; DeVoe, D. L.; Gaitan, M. "Microfluidic Mixing and the Formation Mechanism of Nanoscale Lipid Vesicles." *Manuscript submitted for publication.* **2009**.

[83] Korgel, B. A.; van Zanten, J. H.; Monbouquette, H. G. "Vesicle size distributions measured by flow field-flow fractionation coupled with multiangle light scattering." *Biophysical Journal* **1998**, *74*, 3264-3272.

[84] Strand, B. L.; Morch, Y. A.; Espevik, T.; Skjak-Braek, G. "Visualization of alginate-poly-L-lysine-alginate microcapsules by confocal laser scanning microscopy." *Biotechnology and Bioengineering* **2003**, *82*, 386-394.

[85] Stefansson, M. "Assessment of alginic acid molecular weight and chemical composition through capillary electrophoresis." *Analytical Chemistry* **1999**, *71*, 2373-2378.

[86] Torchilin, V. P. "Multifunctional nanocarriers." *Advanced Drug Delivery Reviews* **2006**, *58*, 1532-1555.

[87] Agrawal, A.; Deo, R.; Wang, G. D.; Wang, M. D.; Nie, S. M. "Nanometer-scale mapping and single-molecule detection with color-coded nanoparticle probes." *Proceedings of the National Academy of Sciences* **2008**, *105*, 3298-3303.

[88] Hu, Z. B.; Lu, X. H.; Gao, J.; Wang, C. J. "Polymer gel nanoparticle networks." *Advanced Materials* **2000**, *12*, 1173-1176.

[89] Kim, J. S.; Rieter, W. J.; Taylor, K. M. L.; An, H.; Lin, W. L.; Lin, W. B. "Self-assembled hybrid nanoparticles for cancer-specific multimodal imaging." *Journal of the American Chemical Society* **2007**, *129*, 8962-8963.

[90] Fenart, L.; Casanova, A.; Dehouck, B.; Duhem, C.; Slupek, S.; Cecchelli, R.; Betbeder, D. "Evaluation of effect of charge and lipid coating on ability of 60-nm nanoparticles to cross an in vitro model of the blood-brain barrier." *Journal of Pharmacology and Experimental Therapeutics* **1999**, *291*, 1017-1022.

[91] Lewinski, N.; Colvin, V.; Drezek, R. "Cytotoxicity of nanoparticles." *Small* **2008**, *4*, 26-49.

[92] Ferdous, A. J.; Stembridge, N. Y.; Singh, M. "Role of monensin PLGA polymer nanoparticles and liposomes as potentiator of ricin A immunotoxins in vitro." *Journal of Controlled Release* **1998**, *50*, 71-78.

[93] An, S. Y.; Bui, M. P. N.; Nam, Y. J.; Han, K. N.; Li, C. A.; Choo, J.; Lee, E. K.; Katoh, S.; Kumada, Y.; Seong, G. H. "Preparation of monodisperse and size-controlled poly(ethylene glycol) hydrogel nanoparticles using liposome templates." *Journal of Colloid and Interface Science* **2009**, *331*, 98-103.

[94] Kabanov, A. V.; Vinogradov, S. V. "Nanogels as Pharmaceutical Carriers: Finite Networks of Infinite Capabilities." *Angewandte Chemie-International Edition* **2009**, *48*, 5418-5429.

[95] Xu, Q. B.; Hashimoto, M.; Dang, T. T.; Hoare, T.; Kohane, D. S.; Whitesides, G. M.; Langer, R.; Anderson, D. G. "Preparation of Monodisperse Biodegradable Polymer Microparticles Using a Microfluidic Flow-Focusing Device for Controlled Drug Delivery." *Small* **2009**, *5*, 1575-1581.

[96] Jiang, W.; Kim, B. Y. S.; Rutka, J. T.; Chan, W. C. W. "Nanoparticle-mediated cellular response is size-dependent." *Nature Nanotechnology* **2008**, *3*, 145-150.

[97] Wong, H. L.; Bendayan, R.; Rauth, A. M.; Wu, X. Y. "Development of solid lipid nanoparticles containing lonically complexed chemotherapeutic drugs and chemosensitizers." *Journal of Pharmaceutical Sciences* **2004**, *93*, 1993-2008.

[98] Liu, J. W.; Stace-Naughton, A.; Jiang, X. M.; Brinker, C. J. "Porous Nanoparticle Supported Lipid Bilayers (Protocells) as Delivery Vehicles." *Journal of the American Chemical Society* **2009**, *131*, 1354-+.

[99] Hong, J. S.; Vreeland, W. N.; DePaoli Lacerda, S. H.; Locascio, L. E.; Gaitan, M.; Raghavan, S. R. "Liposome-templated supramolecular assembly of responsive alginate nanogels." *Langmuir* **2008**, *24*, 4092-4096.

[100] "Certain commercial materials and equipment and identified in order to specify adequately experimental procedures. In no case does such identification imply recommendation or endorsement by the Nationals Institute of Standards and Technology, not does it imply that the items identified are necessarily the best available for the puropose.".

[101] Moghimi, S. M.; Hunter, A. C.; Murray, J. C. "Long-circulating and target-specific nanoparticles: Theory to practice." *Pharmacological Reviews* **2001**, *53*, 283-318.

[102] Zangmeister, R. A.; Tarlov, M. J. "UV graft polymerization of polyacrylamide hydrogel plugs in microfluidic channels." *Langmuir* **2003**, *19*, 6901-6904.

[103] Vermonden, T.; Fedorovich, N. E.; van Geemen, D.; Alblas, J.; van Nostrum, C. F.; Dhert, W. J. A.; Hennink, W. E. "Photopolymerized thermosensitive hydrogels: Synthesis, degradation, and cytocompatibility." *Biomacromolecules* **2008**, *9*, 919-926.

[104] Sabnis, A.; Rahimi, M.; Chapman, C.; Nguyen, K. T. "Cytocompatibility studies of an in situ photopolymerized thermoresponsive hydrogel nanoparticle system using human aortic smooth muscle cells." *Journal of Biomedical Materials Research Part A* **2009**, *91A*, 52-59.

[105] Fedorovich, N. E.; Oudshoorn, M. H.; van Geemen, D.; Hennink, W. E.; Alblas, J.; Dhert, W. J. A. "The effect of photopolymerization on stem cells embedded in hydrogels." *Biomaterials* **2009**, *30*, 344-353.

[106] Bryant, S. J.; Nuttelman, C. R.; Anseth, K. S. "Cytocompatibility of UV and visible light photoinitiating systems on cultured NIH/3T3 fibroblasts in vitro." *Journal of Biomaterials Science-Polymer Edition* **2000**, *11*, 439-457.

[107] Williams, C. G.; Malik, A. N.; Kim, T. K.; Manson, P. N.; Elisseeff, J. H. "Variable cytocompatibility of six cell lines with photoinitiators used for polymerizing hydrogels and cell encapsulation." *Biomaterials* **2005**, *26*, 1211-1218.

[108] Ramanan, R. M. K.; Chellamuthu, P.; Tang, L. P.; Nguyen, K. T. "Development of a temperature-sensitive composite hydrogel for drug delivery applications (vol 22, pg 120, 2006)." *Biotechnology Progress* **2006**, *22*, 1464-1464.